Scholars' Mine

Doctoral Dissertations

Student Theses and Dissertations

2014

Automated classification of malignant melanoma based on detection of atypical pigment network in dermoscopy images of skin lesions

Nabin K. Mishra

Follow this and additional works at: https://scholarsmine.mst.edu/doctoral_dissertations

Part of the Computer Sciences Commons, Electrical and Computer Engineering Commons, and the Oncology Commons

Department: Electrical and Computer Engineering

AUTOMATED CLASSIFICATION OF MALIGNANT MELANOMA BASED ON

DETECTION OF ATYPICAL PIGMENT NETWORK IN DERMOSCOPY IMAGES

OF SKIN LESIONS

by

NABIN KUMAR MISHRA

A DISSERTATION

Presented to the Faculty of the Graduate School of the

MISSOURI UNIVERSITY OF SCIENCE AND TECHNOLOGY

In Partial Fulfillment of the Requirements for the Degree

DOCTOR OF PHILOSOPHY

in

ELECTRICAL ENGINEERING

2014

Approved by:

Dr. Randy H. Moss, Advisor
Dr. William V. Stoecker
Dr. Bijaya Shrestha
Dr. R. J. Stanley
Dr. Steve Grant

PUBLICATION DISSERTATION OPTION

This dissertation has been prepared in the style utilized by the Missouri University of Science and Technology and consists of three articles. The first paper titled "Automatic Dermoscopy Skin Lesion Border Classification" in pages 7 through 31 is prepared and ready to be submitted for publication. The second paper titled "Segmentation of Atypical Pigment Network in Skin Lesion Images and Classification of Melanoma Using Features Extracted from the Segmented Regions" in pages 32 through 58 is prepared and ready to be submitted for publication. The third paper titled "Automated Classification of Malignant Melanoma Using Fusion of Clinical and Dermoscopy Features from Skin Lesion Images" in pages 59 through 82 is prepared and ready to be submitted for publication.

ABSTRACT

Melanoma causes more deaths than any other form of skin cancer. Early melanoma detection is important to prevent progression to a more deadly stage. Automated computer-based identification of melanoma from dermoscopic images of skin lesions is the most efficient method in early diagnosis. An automated melanoma identification system must include multiple steps, involving lesion segmentation, feature extraction, feature combination and classification. In this research, a classifier-based approach for automatically selecting a lesion border mask for segmentation of dermoscopic skin lesion images is presented. A logistic regression based model selects a single lesion border mask from multiple border masks generated by multiple lesion segmentation algorithms. This research also presents a method of segmenting atypical pigment network (APN) based on variance in the red plane in the lesion area of a dermoscopic image. Features extracted from APN regions are used in automated classification of melanoma. The automated identification of melanoma is further improved by fusion of other features relevant to melanoma detection. This research uses clinical features, APN features, median split cluster features, pink area features, white area features and salient point features in various hierarchical combinations to improve the overall performance in melanoma identification. A training set of 837 dermoscopic skin lesion images together with a disjoint test set of 804 dermoscopic skin lesion images are used in this research to produce the experimental findings.

ACKNOWLEDGMENTS

TABLE OF CONTENTS

LIST OF ILLUSTRATIONS

LIST OF TABLES

SECTION

1. INTRODUCTION

1.1. BACKGROUND

Skin cancer is a very common type of cancer among both sexes in the United States. Among different types of skin cancer, malignant melanoma is considered to be the deadliest and is responsible for the most skin cancer deaths [1]. An estimated 76,100 new melanomas will be diagnosed and about 9,710 people are expected to die of melanoma during the year 2014 in the United States [1]. Failure to diagnose melanoma in its earlier stage may allow it to be lethal, hence its early detection is critically important to reduce deaths caused by melanoma. However, decisions made by professionals in the area for diagnosis of melanoma are very subjective and they often have to depend on pathological tests which take time. Due to high subjectivity and dependence on pathological tests, numerous unnecessary biopsies are performed every year. Over a billion dollars per year is spent on biopsying lesions that turn out to be benign, and even then cases of melanoma are missed by domain experts [2]. Hence, the need for a computer-aided system has risen significantly as professionals are seeking assistance in faster and accurate diagnosis of melanoma in replacement of time consuming, invasive and expensive methods. Any such novel computer-aided system or algorithm has to be highly accurate in order to be implemented consistently in the diagnostic process. Assisting in the development of such a computer-aided system is a method called dermoscopy.

1.2. RESOURCE, DATA AND TOOLS

Dermoscopy, a technical name for epiluminescence light microscopy (ELM), is a non-invasive technique that magnifies the lesion and enables visibility of subsurface structures, improving in vivo diagnosis of pigmented skin lesions [3-4]. In particular, contact non-polarized dermoscopy, a variant of dermoscopy that combines optical magnification and liquid immersion to make subsurface lesion features visible, is widely used in the diagnosis of melanoma [5]. It is also anticipated that advances in this technology will allow improved detection of melanoma in the early stage. With such vision, numerous image analysis techniques have been developed using contact non-polarized dermoscopy to detect structures and segments such as white areas [6], atypical pigment network (APN) [7], median split color segments [8], pink areas [9] and salient points [10] among others, which are significant in melanoma identification. Various lesion segmentation algorithms are also developed to aid in segmentation of such structures and regions [11].

This research work is based on a total of 1641 contact non-polarized dermoscopy images divided into a training set of 837 dermoscopy images and a disjoint test set of 804 dermoscopy images. These images were obtained from four clinics during the years 2007 to 2009. They were acquired by similar processes using similar lighting and at similar magnification levels.

Segmentation algorithms used in this research are developed in MATLAB® (various versions), The Mathworks Inc., 3 Apple Hill Drive, Natick, MA 01760-2098, USA and in C++ in combination with the open source computer vision library OpenCV. Classifier models used in this research are based on logistic regression and are developed

using SAS® 9.1, SAS Institute Inc., 100 SAS Campus Drive, Cary, NC 27513-2414, USA.

1.3. RESEARCH CONTRIBUTIONS

This dissertation consists of research contributions in the following three areas of automated classification of melanoma:

1. Automatic dermoscopy skin lesion border classification

2. Segmentation of atypical pigment network in skin lesion images and classification of melanoma using features extracted from the segmented regions

3. Automated classification of malignant melanoma using fusion of clinical and dermoscopy features extracted from skin lesion images

An accurate skin lesion segmentation is the first step in any automatic analysis of a dermoscopy image for proper diagnosis of a lesion type. Due to the variation in skin color, skin condition, lesion type and lesion area, automatic segmentation algorithms are not successful enough to generate an accurate segmentation of skin lesion. Hence, an automatic lesion border classifier is presented in this research which identifies a good lesion border among different choices available from different segmentation algorithms, thereby increasing the overall performance of generating an accurate lesion border for melanoma classification.

Atypical pigment networks are brown, black or gray meshes or thick lines in dermoscopy images [12]. This research presents a method of segmentation of APN regions based on variance in the red plane. Features are then extracted from the segmented APN and non-APN regions to build a classifier model for detection of melanoma.

In addition to the APN features, this research also uses features generated from other significant structures and regions like pink areas, white areas, salient points and median split color segments, along with clinical features to generate models for classification of melanoma. Various models are generated based on different combinations of features in a two-step hierarchical melanoma classifier model. It demonstrates the potential of feature combinations at different steps for accurate classification of melanoma.

1.4. DISSERTATION OUTLINE

The contribution and results of this research are compiled as three chapters in this dissertation. Automatic dermoscopy skin lesion border classification is presented in Chapter I. Segmentation of atypical pigment network in skin lesion images and classification of melanoma using features extracted from the segmented regions is presented in Chapter II. Automated classification of malignant melanoma using fusion of clinical and dermoscopy features extracted from skin lesion images is presented in Chapter III.

REFERENCES

1. Siegel, Rebecca, Jiemin Ma, Zhaohui Zou, and Ahmedin Jemal. "Cancer statistics, 2014." *CA: A Cancer Journal for Clinicians* 64, no. 1 (2014): 9-29.

2. "The Cost of Cancer." National Cancer Institute at the National Institutes of Health. 2011. *http://www.cancer.gov/aboutnci/servingpeople/ understanding burden/costofcancer*.

3. Argenziano, Giuseppe, H. Peter Soyer, Sergio Chimenti, Renato Talamini, Rosamaria Corona, Francesco Sera, Michael Binder, Lorenzo Cerroni, Gaetano De Rosa, Gerardo Ferrara, Rainer Hofmann-Wellenhof, Michael Landthaler, Scott W. Menzies, Hubert Pehamberger, Domenico Piccolo, Harold S. Rabinovitz, Roman Schiffner, Stefania Staibano, Wilhelm Stolz, Igor Bartenjev, Andreas Blum, Ralph Braun, Horacio Cabo, Paolo Carli, Vincenzo De Giorgi, Matthew G. Fleming, James M. Grichnik, Caron M. Grin, Allan C. Halpern, Robert Johr, Brian Katz, Robert O. Kenet, MD, Harald Kittler, Jürgen Kreusch, Josep Malvehy, Giampiero Mazzocchetti, Margaret Oliviero, Fezal Özdemir, Ketty Peris, Roberto Perotti, Ana Perusquia, Maria Antonietta Pizzichetta, Susana Puig, Babar Rao, Pietro Rubegni, Toshiaki Saida, Massimiliano Scalvenzi, Stefania Seidenari, Ignazio Stanganelli, Masaru Tanaka, Karin Westerhoff, Ingrid H. Wolf, Otto Braun-Falco, Helmut Kerl, Takeji Nishikawa, Klaus Wolff, Alfred W. Kopf. "Dermoscopy of pigmented skin lesions: results of a consensus meeting via the Internet." *Journal of the American Academy of Dermatology* 48, no. 5 (2003): 679-693.

4. Argenziano, Giuseppe, H. Peter Soyer, Vincenzo De Giorgio, Domenico Piccolo, Paolo Carli, Mario Delfino, Angela Ferrari, Rainer Hofmann-Wellenhof, Daniela Massi, Giampero Mazzocchetti, Massimiliano Scalvenzi, Ingrid H. Wolf. "Interactive atlas of dermoscopy." *Edra Medical Publishing & New Media*, Milan, Italy, 2000.

5. Sforza, Gianluca, Giovanna Castellano, S. A. Arika, Robert W. LeAnder, R. Joe Stanley, William V. Stoecker, and Jason R. Hagerty. "Using Adaptive Thresholding and Skewness Correction to Detect Gray Areas in Melanoma In Situ Images." *IEEE Transactions on Instrumentation and Measurement* 61, no. 7 (2012): 1839-1847.

6. Dalal, Ankur, Randy H. Moss, R. Joe Stanley, William V. Stoecker, Kapil Gupta, David A. Calcara, Jin Xu, Bijaya Shrestha, Rhett Drugge, Joseph M. Malters, Lindall A. Perry. "Concentric decile segmentation of white and hypopigmented areas in dermoscopy images of skin lesions allows discrimination of malignant melanoma." *Computerized Medical Imaging and Graphics* 35, no. 2 (2011): 148-154.

7.   Shrestha, Bijaya, Joseph Bishop, Keong Kam, Xiaohe Chen, Randy H. Moss, William V. Stoecker, Scott Umbaugh, R. Joe Stanley, M. Emre Celebi, Ashfaq A. Marghoob, Giuseppe Argenziano, H. Peter Soyer. "Detection of atypical texture features in early malignant melanoma." *Skin Research and Technology* 16, no. 1 (2010): 60-65.

8.   Ghantasala, Kaushik. "Feature extraction through median-split algorithm for melanoma detection." M.S. Thesis in Electrical Engineering, Missouri University of Science & Technology, Rolla, MO, USA, 2013.

9.   Rader, Ryan K., Katie S. Payne, Uday Guntupalli, Harold S. Rabinovitz, Maggie C. Oliviero, Rhett J. Drugge, Joseph J. Malters, and William V. Stoecker. "The Pink Rim Sign: Location of Pink as an Indicator of Melanoma in Dermoscopic Images." *Journal of Skin Cancer* vol. 2014, Article ID 719740, 7 pages, (2014).

10.   Jella, Pavani. "Pigment network extraction and salient point analysis." M.S. Thesis in Electrical Engineering, University of Missouri, Rolla, MO, USA, 2004.

11.   Celebi, M. Emre, Hitoshi Iyatomi, Gerald Schaefer, and William V. Stoecker. "Lesion border detection in dermoscopy images." *Computerized Medical Imaging and Graphics* 33, no. 2 (2009): 148-153.

12.   Perrinaud, A., O. Gaide, L. E. French, J-H. Saurat, A. A. Marghoob, and R. P. Braun. "Can automated dermoscopy image analysis instruments provide added benefit for the dermatologist? A study comparing the results of three systems." *British Journal of Dermatology* 157, no. 5 (2007): 926-933.

PAPER

I. AUTOMATIC DERMOSCOPY SKIN LESION BORDER CLASSIFICATION

Nabin K. Mishra[a], Randy H. Moss[a], Ravneet Kaur[b], Reda Kasmi[c], Justin G. Cole[d], William V. Stoecker[d,e]

[a]Department of Electrical and Computer Engineering, Missouri University of Science and Technology (S&T), Rolla, MO, 65409, USA

[b]Department of Electrical and Computer Engineeering, Southern Illinois University Edwardsville, Edwardsville, IL, 62026, USA

[c]University of Bejaia, Bejaia, Algeria

[d]Stoecker & Associates, Rolla, MO, 65401, USA

[e]Department of Dermatology, University of Missouri School of Medicine, Columbia, MO, 65212, USA

ABSTRACT

This paper presents a classifier-based approach for automatically selecting a lesion border mask for dermoscopic skin lesion images. The variation in morphology and color of dermoscopic skin lesion images makes segmentation of skin lesions a difficult problem. The accuracy of a single algorithm to provide an acceptable lesion border is not high enough to assist in any further processing of skin lesions. In this paper, a logistic regression-based lesion border classifier model is presented. This model selects a single lesion border from multiple borders generated by multiple lesion segmentation algorithms, jointly providing an acceptable border for a given set of images. Features used to build the model are based on morphology of the automatic lesion border and the color variations inside and outside of the lesion. The overall performance of the

classifier-based automatic skin lesion finder is found to be better than any single algorithm used in this research.

1. INTRODUCTION

Melanoma is the deadliest form of skin cancer, causing a large majority of skin cancer deaths. It is estimated that about 76,100 new melanomas will be diagnosed and about 9,710 people are expected to die of melanoma in the United States in the year 2014 [1]. It is fully curable if diagnosed in its earlier stage. Over a billion dollars per year is spent on biopsying lesions that turn out to be benign, and even then cases of melanoma are missed by domain experts [2].

The dermoscopy imaging method has been very popular in recent years in skin cancer diagnosis. This method has been reported to be a very important tool in the early detection of melanoma [3-6]. Studies have shown that dermoscopy increases the diagnostic accuracy over clinical visual inspection in the hands of experienced physicians [7-9]. Hence automatic analysis of lesion dermoscopy has been an area of research in recent years.

Skin lesion segmentation is the first step in any automatic analysis of a dermoscopy image. Hence, an accurate lesion segmentation algorithm is essential for the proper diagnosis of lesion type. Numerous research papers have been published describing a variety of lesion segmentation algorithms [10-29]. Each of those algorithms has its own advantages and disadvantages; each performing well on certain sets of images. But with the variety in skin color, skin condition, lesion type and lesion area, those algorithms are not capable of providing the proper segmentation of a skin lesion

every time. Incapability of the lesion segmentation algorithms to provide a perfect lesion segmentation leads to this idea of incorporating multiple lesion segmentation algorithms, with different algorithms working best in different types of lesion and skin conditions, into a single system. This system would be able to provide a good segmentation of a lesion by selecting the best among the multiple choices obtained from multiple algorithms. Hence, this novel idea of implementing a lesion border classifier to solve the border selection problem is proposed.

In this paper, an automatic dermoscopy skin lesion border classifier is presented, which will select the best lesion border among the choices available for any skin lesion. Figure 1 illustrates a basic block diagram of the proposed automatic border classifier. This border classifier uses morphological and color features from the segmented border and the dermoscopy image to select the best border among different available choices.

The rest of the paper is organized as follows. Section 2 explains about the segmentation algorithms used in this research. Section 3 explains different features used in the classifier. Section 4 describes the classifier setup. Section 5 discusses the result. Finally, section 6 gives the conclusion and possible future work.
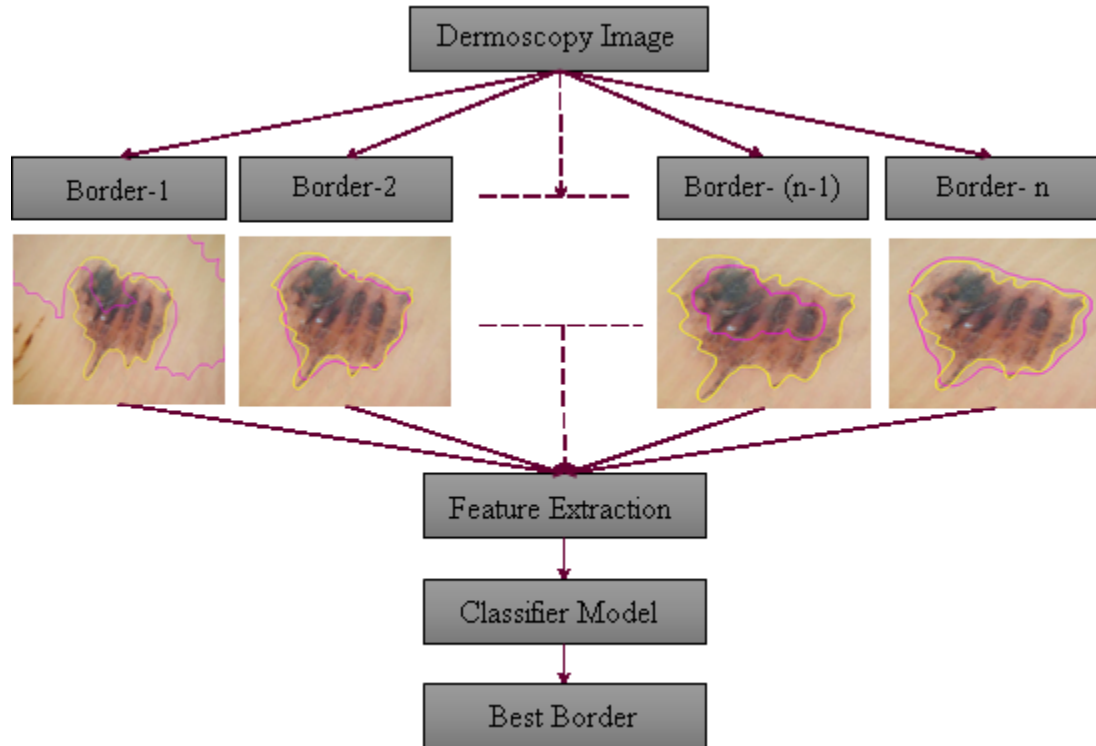
Figure 1. Block diagram of the lesion border classifier, computer-generated border shown in red; correct border shown in yellow for comparison.

2. SEGMENTATION ALGORITHMS

A total of fifteen different segmentation algorithms are currently used in this research to build a classifier model. These algorithms are selected and developed based on their performance on different types of skin lesion images rather than their overall accuracy on the available image set. Each algorithm produces a good border for certain types of skin lesions, with some being better on multiple lesion types which hence have better overall accuracy. A single algorithm with the highest overall accuracy is still not enough for providing good segmentation on all images selected for the experiment. A

single border for each image, manually drawn by a dermatologist, is also used in building the classifier model.

Seven of the border segmentation algorithms are based on geodesic active contour (GAC), implemented using the level set algorithm [30-32]. The initial contour is found by segmentation of a pre-processed image, using a modified Otsu threshold [15]. Based on seven different pre-processing methods performed on the RGB dermoscopy image, seven different borders are obtained using GAC and the level set algorithm. Histogram thresholding applied separately on a smoothed blue color plane and on a pink-chromaticity image provide another two different lesion borders [10, 33]. An image thresholding method based on minimizing the measures of fuzziness of a dermoscopy skin lesion image is used as another method of segmenting a skin lesion [34, 35]. The next skin lesion segmentation algorithm is based on minimum cross entropy thresholding where threshold selection is performed by minimizing the cross entropy between the dermoscopy image and its segmented version [35-36]. Next, a more pertinent information measure of an image is obtained by modifying an entropy method for image thresholding to obtain two more lesion borders by applying different pre-processing and post-processing methods [35, 37]. Last two segmentation algorithms are based on the principal components transform (PCT) and the median split algorithm [38]. An RGB image is first transformed using the PCT and then a median split is performed on the transformed image to obtain the lesion border mask. Two different masks using this method are obtained by two different post-processing approaches. In addition, one manually drawn border for each image is also used for training the classifier.

3. FEATURE DESCRIPTION

The proposed lesion border classifier uses morphological features calculated from the candidate lesion borders and color features calculated from the dermoscopy image to identify the best border among the choices available. There are seven morphological and forty-eight color-related features used in the classification process.

3.1. MORPHOLOGICAL FEATURES

This section explains various morphological features used in this research.

(a) Centroid location: Centroid location is the location of the centroid of the area enclosed by the lesion border in terms of its x and y coordinates of the pixel location with the origin being at the upper left corner of the image. Centroid location, in terms of x and y coordinates of a collection of pixels are given by the following equations,

$$\overline{X_c} = \frac{1}{n} \sum_{i=1}^{n} x_i \tag{1}$$

$$\overline{Y_c} = \frac{1}{n} \sum_{i=1}^{n} y_i \tag{2}$$

where n is the number of pixels in the lesion area, x_i is the x coordinate of the ith pixel and y_i is the y coordinate of the ith pixel.

(b) Centroid distance (D_c): Centroid distance is the distance between the centroid of the image and the centroid of the lesion border. It is calculated as follows

$$D_c = \sqrt{(x_{c,lb} - x_{c,im})^2 + (y_{c,lb} - y_{c,im})^2} \tag{3}$$

where $(x_{c,lb}, y_{c,lb})$ is lesion border centroid and $(\boldsymbol{x_{c,im}}, \boldsymbol{y_{c,im}})$ is image centroid; which is the center of the image.

(c) Lesion perimeter (*LP*): Lesion perimeter is calculated by counting the outermost pixels of the lesion.

(d) Lesion area (*LA*): Lesion area is calculated by counting the number of pixels inside the lesion border.

(e) Scaled centroid distance (*SD$_c$*): Scaled centroid distance is the ratio of centroid distance (*D$_c$*) to the square root of lesion area and is given by

$$SD_c = \frac{D_c}{\sqrt{LA}} \tag{4}$$

(f) Compactness (*C*): Compactness is defined as the ratio of the lesion perimeter to the square root of 4π times the lesion area. This measure compares the object with a circle whose compactness is unity. It is calculated as shown in Eq. (5).

$$C = \frac{LP}{\sqrt{4 * \pi * LA}} \tag{5}$$

3.2. COLOR FEATURES

Color features are calculated separately from different target areas in the image. Target areas are defined with an intention to identify the color difference between the inside and outside of the lesion. Some of the targeted areas are selected by calculating the distance transform of the binary lesion border image. The selected target areas are defined below and are shown in Figure 2.

• Inside lesion area: It is the region inside the lesion border as shown in Figure 2(a). It is the same as the lesion area.

• Outside lesion area: It is the region outside the lesion border that extends to the image boundary as shown in Figure 2(b). If the lesion border covers the entire image,

then the outside lesion area is represented as zero and hence all the color features in this region are represented by zero.

• Rim area outside lesion border: It is the region just outside the lesion border. The distance transform matrix is used to select pixels in this region. Any pixels within the distance of $50\sqrt{2}(\approx 70.71)$ from the lesion boundary are selected to be in this region. This region is shown in Figure 2(c).

• Rim area inside lesion border: It is a region just inside the lesion border. In this case as well, the distance transform matrix is used to select pixels in the region. Any pixels within the distance of $50\sqrt{2}(\approx 70.71)$ from the lesion boundary is selected to be in this region as shown in Figure 2(d).

• Overlapping rim area at lesion border: It is a region that covers a portion of area just outside the lesion boundary and another portion just inside the lesion boundary. The distance transform is calculated from the lesion boundary going outside the lesion and inside the lesion. Any pixels within the distance of $0.75 * 50\sqrt{2}(\approx 50.03)$ is selected to be in this region. This region is illustrated in the Figure 2(e).

(a) Inside lesion area   (b) Outside lesion area   (c) Outer rim area

(d) Inner rim area   (e) Overlapping rim area
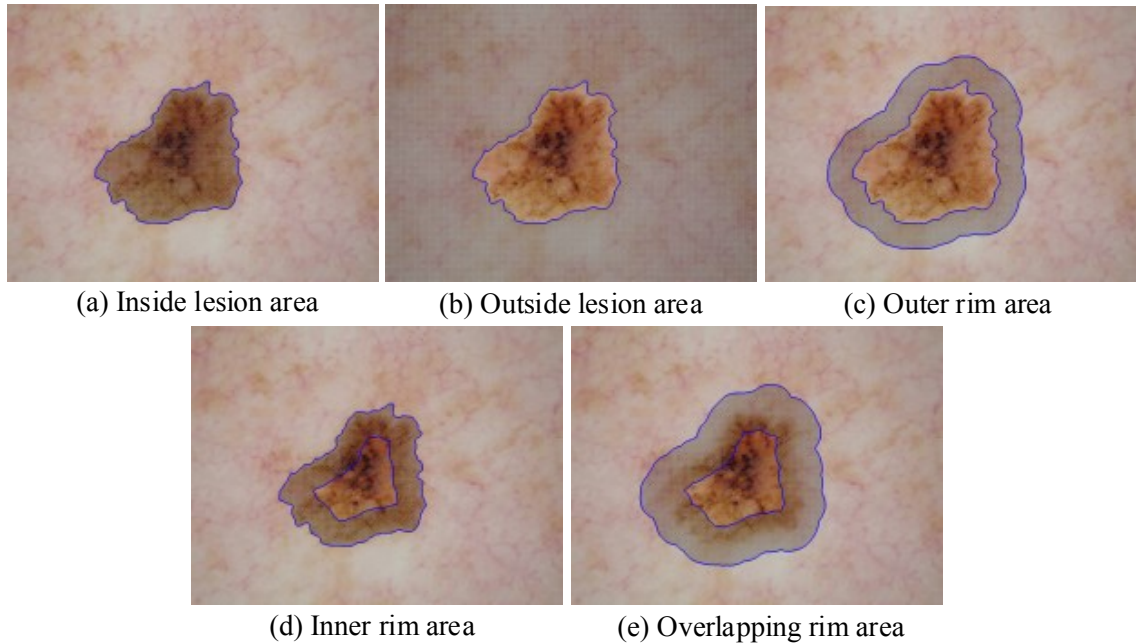
Figure 2. Target areas for extraction of color features are highlighted in shades.

In calculating the color features, regions of dark corners are excluded. A dark corner is defined as a region, within a distance of 250 pixels from a corner of the image, where the intensity value of a grayscale image is less than 75. This is determined by performing histogram analysis of samples with dark corners in the training and the test set. If any holes exist in that region then they are filled. A sample image with dark corners in the upper left, upper right and lower left corners is shown in Figure 3(a) and the dark corner mask is shown in Figure 3(b).

| (a) Original lesion image | (b) Dark corner mask |
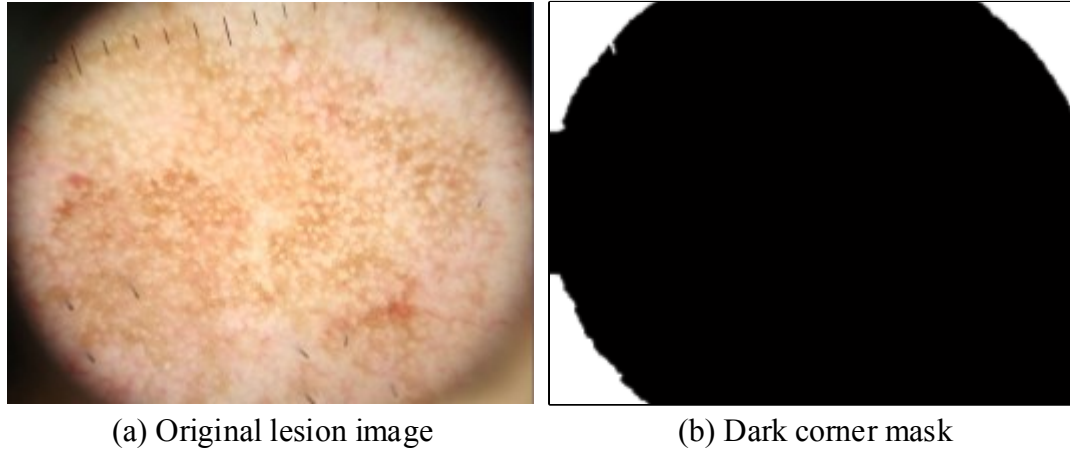
Figure 3. Sample dark corner image and its dark corner mask (shown in white).

The dark corner mask is used along with the original border mask to obtain an effective border in order to calculate the color features excluding the dark corners since they are not part of the lesion but part of the camera setup. The effective border mask is obtained by performing logical operations as shown in Eq. (6) and Eq. (7), and is illustrated in Figure 4(a) and Figure 4(b).

$$M_{commA} = M_{dc} \wedge M_{region} \tag{6}$$

$$M_{effR} = M_{commA} \oplus M_{border} \tag{7}$$

where, M_{dc}: dark corner mask.

M_{region}: region mask (any one of the five possible regions).

M_{commA}: intermediate mask that represents the common area between the dark corner and the selected region.

M_{effR}: effective region mask

$\wedge$: represents logical AND operation

$\oplus$: represents logical exclusive-OR (XOR) operation

| dark corner mask | lesion border mask | common area after AND operation | effective lesion border mask |

(a)

| dark corner mask | outside lesion mask | common area after AND operation | effective lesion outside area |

(b)
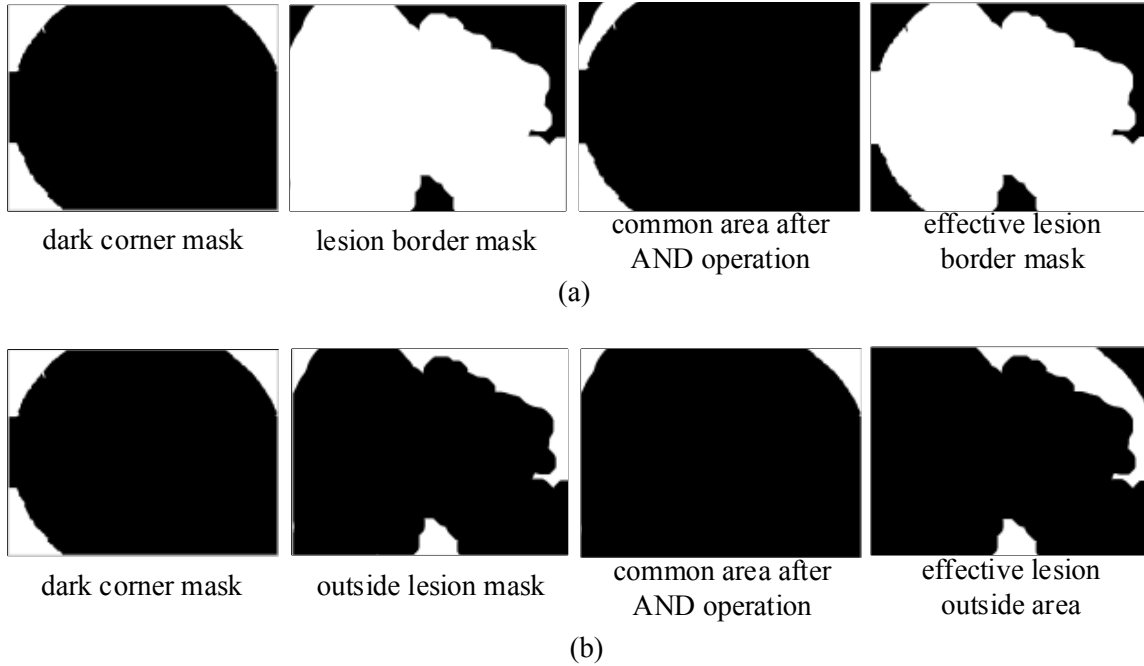
Figure 4. Exclusion of dark corner region by logical operations.

The operations in Eq. (6) and Eq. (7) are performed for all the five regions shown in Figure 2. The color features are then calculated over the effective region for all five different regions. The color features used in the research area are as follows.

(a) Mean intensity of red, green and blue color planes for each effective region: The red, the green and the blue intensity planes from the dermoscopy image are used along with the individual effective region masks to calculate the mean intensity of red, green and blue color planes as shown in Eq. (8), Eq. (9) and Eq. (10) respectively.

$$\overline{R_{effR}} = \frac{1}{N} \sum_{i=1}^{N} I_{red}(i) \tag{8}$$

$$\overline{G_{effR}} = \frac{1}{N}\sum_{i=1}^{N} I_{green}(i) \tag{9}$$

$$\overline{B_{effR}} = \frac{1}{N}\sum_{i=1}^{N} I_{blue}(i) \tag{10}$$

where I_{red}, I_{green} and I_{blue} represent the intensity of red, green and blue color planes, respectively, and N represents the total number of pixels in the effective region.

(b) Intensity standard deviation of red, green and blue planes for each effective region: After calculating the mean intensity of each color plane for each effective region, intensity standard deviation is calculated for the same using Eq. (11), Eq. (12) and Eq. (13).

$$stdR_{effR} = \sqrt{\frac{1}{N-1}\sum_{i=1}^{N}\left(I_{red}(i) - \overline{R_{effR}}\right)^2} \tag{11}$$

$$stdG_{effR} = \sqrt{\frac{1}{N-1}\sum_{i=1}^{N}\left(I_{green}(i) - \overline{G_{effR}}\right)^2} \tag{12}$$

$$stdB_{effR} = \sqrt{\frac{1}{N-1}\sum_{i=1}^{N}\left(I_{blue}(i) - \overline{B_{effR}}\right)^2} \tag{13}$$

where I_{red}, I_{green} and I_{blue} represent the intensity of red, green and blue color planes, respectively. $\overline{R_{effR}}$, $\overline{G_{effR}}$ and $\overline{B_{effR}}$ represent the mean intensity of red, green and blue planes, respectively, for the effective region. N represents the total number of pixels in the effective region.

(c) Mean intensity and standard deviation of grayscale image for each effective region: In order to calculate these features, the grayscale image is obtained by using Eq. (14). The

grayscale image is then used to calculate the mean intensity of grayscale image and the

standard deviation of grayscale image using Eq. (15) and Eq. (16), respectively.

$$I_{gray}(r,c) = 0.2989 * I_{red}(r,c) + 0.5870 * I_{green}(r,c) + 0.1140 * I_{blue}(r,c) \quad (14)$$

$$\overline{Gray_{effR}} = \frac{1}{N}\sum_{i=1}^{N} I_{gray}(i) \quad (15)$$

$$stdGray_{effR} = \sqrt{\frac{1}{N-1}\sum_{i=1}^{N}\left(I_{gray}(i) - \overline{Gray_{effR}}\right)^2} \quad (16)$$

(d) Difference of the mean intensity of outer rim and inner rim for effective region: It is

the absolute difference between the mean intensity of the outer rim and the inner rim for

each RGB color plane and the grayscale image.

(e) Difference of the standard deviation of outer rim and inner rim for effective region: It

is the absolute difference between the standard deviation of the outer rim and the inner

rim for each RGB color plane and the grayscale image.

4. EXPERIMENTAL SETUP

4.1. IMAGE DATABASE

A total of 837 dermoscopy images were used for training and 804 dermoscopy

images were used as a disjoint test set in this research. These images were obtained in

four clinics between the years 2007 to 2009. These images were acquired by similar

process using similar lighting and at similar zoom levels.

Each image was run through fifteen different segmentation algorithms which were

discussed briefly in Section 2. In some cases, some of the segmentation algorithms did

not return a lesion border based on size and location filter implemented in the algorithm

itself. One manually obtained lesion border, drawn by a domain expert, was also used from each image in the training set in the process of creating the classifier model. Hence, for the training set with 837 dermoscopy images, a total of 13,086 borders were obtained. Each of these borders were manually rated by a domain expert in one of the following ways:

0 - for being a bad border,

1 - for being a good border and

2 - for being close to a good border (acceptable for melanoma detection).

In order to create a classifier model, only the borders rated as 0 and 1 were used. Hence, a total of 10,770 borders were selected from the 13,086 borders obtained from the training set. In the selected 10,770 borders, there were 4,414 good borders (rated as 1) and 6356 bad borders (rated as 0). The remaining 2,316 borders that were acceptable for melanoma detection (rated as 2) were not used in making the classifier model but were used later during the best border selection process. For each of the lesion borders, 55 different features were calculated.

4.2. CLASSIFIER SETUP

Logistic regression implemented in SAS (SAS Institute Inc., 100 SAS Campus Drive, Cary, NC 27513-2414, USA) was used to build a classifier model for separating good lesion borders and bad lesion borders. It used Chi-Square statistics to determine the significance of the variables, in order to be selected in the model. The stepwise selection method was implemented for selection of the significant features in model building process. In this method, a variable to be added in the model must be statistically significant at a level denoted by SLENTRY. Once the variable is added, stepwise method

looks at all the other variables already included in the model and removes any variable

that are not statistically significant at some level denoted by SLSTAY. Another variable

can only be added after this check is made and the necessary variable removal is

performed. The stepwise process ends when no variable outside the model are

statistically significant at SLENTRY level and every variable in the model is statistically

significant at SLSTAY level. In this research, both the SLENTRY and SLSTAY of 0.11

were used in stepwise selection method of model building. Higher values of SLENTRY

and SLSTAY provides higher accuracy model with less stability while with their lower

values, better stability can be achieved at a cost of a small decrease in performance. The

chosen value here was found to be optimal for the given problem after numerous

experiments.

5. RESULTS AND DISCUSSION

5.1. CLASSIFIER MODEL

The logistic regression procedure generated a model based on training set border

features. Predicting variables and their interactions are selected to be in the model at a

significance level of 0.11 based on their Chi-Square score. The summary of the results

obtained from the model is shown in Table 1. It shows that out of 4414 good borders,

4019 (91.05%) were identified correctly as good and 395 (8.95%) were classified as bad

borders. Similarly, out of 6356 bad borders, 5115 (80.47%) were identified correctly as

bad and 1241 (19.52%) were classified as good. The overall accuracy of the model was

calculated to be 84.8% in terms of being able to distinguish borders used for training.

Table 1. Summary of prediction using the classifier model.

		Predicted Class		
		Good Border	Bad Border	Total
Actual Class	Good Border	4019 (91.05%)	395 (8.95%)	4414
	Bad Border	1241 (19.52 %)	5115 (80.47%)	6356
	Total	5260	5510	10770

Figure 5 shows the receiver operating characteristic (ROC) curve for the lesion

border classifier model for the training set. The area under the ROC curve (AUC) for the

model is 0.949. The vertical axis in the ROC curve represents the sensitivity also called

the true positive rate and the horizontal axis represents the false negative rate which is

obtained by subtracting specificity from unity.
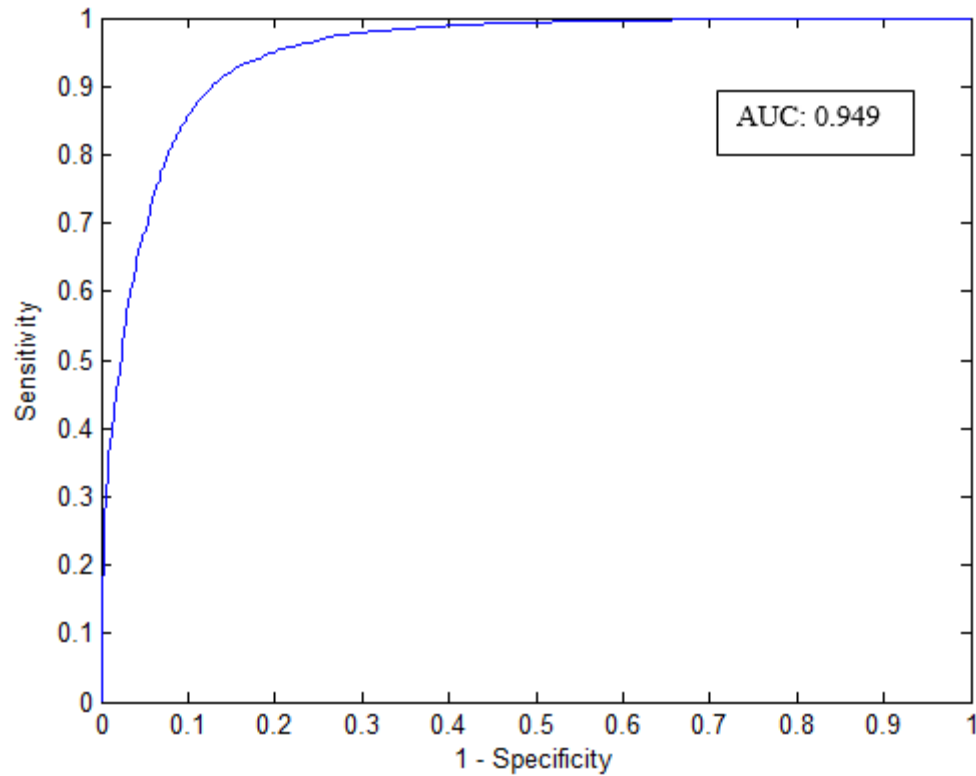
Figure 5. ROC curve for border classifier for the training set.

A generic equation for a model, with n features selected based on the Chi-Sqaure statistic and a certain significance level, obtained from logistic regression is shown in Eq. (17).

$$z = I + \beta_1 * f_1 + \beta_2 * f_2 + \cdots + \beta_n * f_n \tag{17}$$

where I : intercept value from the model

β : estimate value for respective features

f : feature value, it may also represent a combination of features

n : total number of features selected in the model

The *z* value is used to calculated the predicting value, *f(z)*, using Eq. (18), which is the logistic function. The *f(z)* value is used to predict the border either being good or bad.

$$f(z) = \frac{1}{(1 + e^{-z})} \tag{18}$$

5.2. BORDER SELECTION PROCESS

The first step in selecting the best border among different choices available is to calculate *f(z)* value using Eqs. (17) and (18), for each lesion border choice available. The maximum *f(z)* value represents the best border statistically as shown in Eq. (19).

$$LB_{best} = arg \max_{x}\left(f_x(z)\right) \tag{19}$$

where *x* ranges from 1 to 15 representing the number of different segmentation algorithms. Hence, the lesion border with maximum *f(z)* is selected as the best border for any particular skin lesion image.

5.3. OVERALL RESULTS AND ANALYSIS

This section presents the overall accuracy achieved by the classifier model for the training and the test set. The border selection process is performed on both sets. After the best border is selected for each image, each selected border is compared with its corresponding manual rating in order to find the overall success of the classifier model on the training and the test set. For the training set, out of 837 images, 791 best choice lesion borders had a manual rating of either 1 (representing good border) or 2 (representing acceptable border). This means that the classifier model was 94.5% accurate in finding a good or an acceptable border on the training set. It should be noted that borders graded as 2 were not used in generating the classifier model. This accuracy is far better than

76.34%, which is the maximum success rate of a single algorithm among the 15 different methods used in this research applied on the training set.

The best border selection method is also applied on the test set of 804 dermoscopic images. In this case, 743 best choice lesion borders had manual grading of either 1 or 2 (signifying accurate selection) and the remaining 61 best choice lesion borders had manual grading of 0 (signifying not able to find a good border). As a result, the total accuracy of the classifier model on the test set was found to be 92.41%. This accuracy is again better than the most successful single algorithm whose accuracy was 77.74% on the test set. The summary of these results are presented in Table 2.

Table 2. Summary of the lesion border classifier.

Description	Training Set	Test Set
Total number of images	837	804
Number of borders selected with grade 1	611	568
Number of borders selected with grade 2	180	175
Number of borders selected with grade 0	46	61
Classifier accuracy (%)	94.5	92.41
Maximum accuracy with single algorithm (%)	76.34	77.74

This analysis shows that the performance of the automatic border finding system with a logistic regression classifier is approximately 15% more than the best segmentation algorithm used in this research.

6. CONCLUSION AND FUTURE WORK

In this study, a novel approach of automatic lesion border selection for dermoscopy images is presented. This approach involves using a classifier model to select a good lesion border from available multiple lesion segmentation algorithms specializing in segmenting varying lesion types but each with insufficient accuracy. The image sets used in the study were large and the presented overall accuracy of 94.5% for the training set and 91.92% on the test set is significantly better than using any single segmentation algorithm with the highest overall accuracy of 76.34% and 77.74% on the training and the test sets, respectively.

The purpose of the study is to make the analysis of dermoscopy images fully automatic. This method is novel in a way that a classifier is used for selecting the best lesion segment from the existing ones, thereby increasing the overall success. The focus of this study was on the calculation of features and the classification process involving selection of best lesion border. The lesion segmentation and feature generation for classification was fully automatic. The lesion borders were manually rated for the purpose of supervised learning and model creation.

Despite the high accuracy achieved by this method, there is plenty of space for future work. Other classification methods can be explored for better model creation. Some additional features can be studied and incorporated in the classification process.

Instead of only using the border with maximum *f(z)*, the second and the third highest *f(z)* borders can also be reviewed and incorporated or combined using image processing techniques to obtain a better lesion border.

ACKNOWLEDGMENTS

REFERENCES

1. Siegel, Rebecca, Jiemin Ma, Zhaohui Zou, and Ahmedin Jemal. "Cancer statistics, 2014." *CA: A Cancer Journal for Clinicians* 64, no. 1 (2014): 9-29.

2. "The Cost of Cancer." National Cancer Institute at the National Institutes of Health. 2011. *http://www.cancer.gov/aboutnci/servingpeople/understanding-burden/costof cancer.*

3. Pehamberger, Hubert, Michael Binder, Andreas Steiner, and Klaus Wolff. "In vivo epiluminescence microscopy: improvement of early diagnosis of melanoma." *Journal of Investigative Dermatology* 100 (1993): 356S-362S.

4. Soyer, H. Peter, Giuseppe Argenziano, Sergio Chimenti, and Vincenzo Ruocco. "Dermoscopy of pigmented skin lesions." *European Journal of Dermatology* 11, no. 3 (2001): 270-277.

5. Soyer, H. Peter, Giuseppe Argenziano, Renato Talamini, and Sergio Chimenti. "Is dermoscopy useful for the diagnosis of melanoma?" *Archives of Dermatology* 137, no. 10 (2001): 1361-1363.

6. Stolz, Wilhelm, Otto Braun-Falco, Peter Bilek, Michael Landthaler, Walter HC Burgdorf, and Armand B. Cognetta, eds. *Color Atlas of Dermatoscopy*. Wiley-Blackwell, 2002.

7. Braun, Ralph P., Harold S. Rabinovitz, Margeret Oliviero, Alfred W. Kopf, and Jean H. Saurat. "Pattern analysis: a two-step procedure for the dermoscopic diagnosis of melanoma." *Clinics in Dermatology* 20, no. 3 (2002): 236-239.

8. Boldrick, Jennifer C., Christle J. Layton, Josephine Nguyen, and Susan M. Swetter. "Evaluation of digital dermoscopy in a pigmented lesion clinic: clinician versus computer assessment of malignancy risk." *Journal of the American Academy of Dermatology* 56, no. 3 (2007): 417-421.

9. Perrinaud, A., O. Gaide, L. E. French, J-H. Saurat, A. A. Marghoob, and R. P. Braun. "Can automated dermoscopy image analysis instruments provide added benefit for the dermatologist? A study comparing the results of three systems." *British Journal of Dermatology* 157, no. 5 (2007): 926-933.

10. Sahoo, Prasanna K., S. A. K. C. Soltani, and Andrew KC Wong. "A survey of thresholding techniques." *Computer Vision, Graphics, and Image Processing* 41, no. 2 (1988): 233-260.

11. Pal, Nikhil R., and Sankar K. Pal. "A review on image segmentation techniques." *Pattern Recognition* 26, no. 9 (1993): 1277-1294.

12. Silveira, Margarida, Jacinto C. Nascimento, Jorge S. Marques, André RS Marçal, Teresa Mendonça, Syogo Yamauchi, Junji Maeda, and Jorge Rozeira. "Comparison of segmentation methods for melanoma diagnosis in dermoscopy images." *IEEE Journal of Selected Topics in Signal Processing,* 3, no. 1 (2009): 35-45.

13. Celebi, M. Emre, Sae Hwang, Hitoshi Iyatomi, and Gerald Schaefer. "Robust border detection in dermoscopy images using threshold fusion." In *17th IEEE International Conference on Image Processing (ICIP), 2010*, pp. 2541-2544. IEEE, 2010.

14. Taouil, Khaled, and Nadra Ben Romdhane. "Automatic segmentation and classification of skin lesion images." In *The 2nd International Conference on Distributed Frameworks for Multimedia Applications, 2006,* pp. 1-12. IEEE, 2006.

15. Erkol, Bulent, Randy H. Moss, R. Joe Stanley, William V. Stoecker, and Erik Hvatum. "Automatic lesion boundary detection in dermoscopy images using gradient vector flow snakes." *Skin Research and Technology* 11, no. 1 (2005): 17-26.

16. Zhou, Huiyu, Gerald Schaefer, M. Emre Celebi, Faquan Lin, and Tangwei Liu. "Gradient vector flow with mean shift for skin lesion segmentation. "*Computerized Medical Imaging and Graphics* 35, no. 2 (2011): 121-127.

17. Chiem, Andy, Adel Al-Jumaily, and Rami N. Khushaba. "A novel hybrid system for skin lesion detection." In *3rd International Conference on Intelligent Sensors, Sensor Networks and Information, 2007. ISSNIP 2007*, pp. 567-572. IEEE, 2007.

18. Zhou, Huiyu, Gerald Schaefer, Abdul H. Sadka, and M. Emre Celebi. "Anisotropic mean shift based fuzzy c-means segmentation of dermoscopy images." *IEEE Journal of Selected Topics in Signal Processing,* 3, no. 1 (2009): 26-34.

19. Yuan, Xiaojing, Ning Situ, and George Zouridakis. "Automatic segmentation of skin lesion images using evolution strategies." *Biomedical Signal Processing and Control* 3, no. 3 (2008): 220-228.

20. Barcelos, Célia A. Zorzo, and V. B. Pires. "An automatic based nonlinear diffusion equations scheme for skin lesion segmentation." *Applied Mathematics and Computation* 215, no. 1 (2009): 251-261.

21. Yuan, Xiaojing, Ning Situ, and George Zouridakis. "A narrow band graph partitioning method for skin lesion segmentation." *Pattern Recognition* 42, no. 6 (2009): 1017-1028.

22. Mete, Mutlu, Sinan Kockara, and Kemal Aydin. "Fast density-based lesion detection in dermoscopy images." *Computerized Medical Imaging and Graphics* 35, no. 2 (2011): 128-136.

23. Zhou, Huiyu, Xuelong Li, Gerald Schaefer, M. Emre Celebi, and Paul Miller. "Mean shift based gradient vector flow for image segmentation." *Computer Vision and Image Understanding* 117, no. 9 (2013): 1004-1016.

24. Abbas, Qaisar, Irene Fondón, and Muhammad Rashid. "Unsupervised skin lesions border detection via two-dimensional image analysis." *Computer Methods and Programs in Biomedicine* 104, no. 3 (2011): e1-e15.

25. Wang, Hanzheng, Randy H. Moss, Xiaohe Chen, R. Joe Stanley, William V. Stoecker, M. Emre Celebi, Joseph M. Malters, James M. Grichnik, Ashfaq A. Marghoob, Harold S. Rabinovitz, Scott W. Menzies, Thomas M. Szalapski. "Modified watershed technique and post-processing for segmentation of skin lesions in dermoscopy images." *Computerized Medical Imaging and Graphics* 35, no. 2 (2011): 116-120.

26. Celebi, M. Emre, Hitoshi Iyatomi, Gerald Schaefer, and William V. Stoecker. "Lesion border detection in dermoscopy images." *Computerized Medical Imaging and Graphics* 33, no. 2 (2009): 148-153.

27. Zhou, Huiyu, Gerald Schaefer, M. Emre Celebi, Faquan Lin, and Tangwei Liu. "Gradient vector flow with mean shift for skin lesion segmentation." *Computerized Medical Imaging and Graphics* 35, no. 2 (2011): 121-127.

28. Garnavi, Rahil, Mohammad Aldeen, M. Emre Celebi, George Varigos, and Sue Finch. "Border detection in dermoscopy images using hybrid thresholding on optimized color channels." *Computerized Medical Imaging and Graphics* 35, no. 2 (2011): 105-115.

29. Tang, Jinshan. "A multi-direction GVF snake for the segmentation of skin cancer images." *Pattern Recognition* 42, no. 6 (2009): 1172-1179.

30. Kasmi, Reda. Nabin K. Mishra, "Segmenting skin lesions using geodisic active contour." *3rd Quadrennial Automatic Skin Cancer Detection Symposium*, Rolla, MO, USA, 2013.

31. Caselles, Vicent, Ron Kimmel, and Guillermo Sapiro. "Geodesic active contours." *International Journal of Computer Vision* 22, no. 1 (1997): 61-79.

32. Osher, Stanley. James A. Sethian. "Fronts propagating with curvature-dependent speed: algorithms based on Hamilton-Jacobi formulations." *Journal of Computational Physics* 79, no. 1 (1988): 12-49.

33. Szalapski, Thomas M.. Nabin K. Mishra. "Blue plane threshold and pink chromaticity based lesion segmentation." *3rd Quadrennial Automatic Skin Cancer Detection Symposium*, Rolla, MO, USA. 2013.

34. Huang, Liang-Kai. Mao-Jiun J. Wang. "Image thresholding by minimizing the measures of fuzziness." *Pattern Recognition* 28, no. 1 (1995): 41-51.

35. Gabriel Landini. *http://fiji.sc/Auto_Threshold#Li* v1.15, 2013.

36. Li, C. H.. Peter Kwong-Shun Tam. "An iterative algorithm for minimum cross entropy thresholding." *Pattern Recognition Letters* 19, no. 8 (1998): 771-776.

37. Shanbhag, Abhijit G. "Utilization of information measure as a means of image thresholding." *CVGIP: Graphical Models and Image Processing* 56, no. 5 (1994): 414-419.

38. Umbaugh, Scott E. "Segmentation and edge/line detection." *Digital Image Processing and Analysis: Human and Computer Vision Applications with CVIPtools*. CRC press, 2010.

II. SEGMENTATION OF ATYPICAL PIGMENT NETWORK IN SKIN LESION IMAGES AND CLASSIFICATION OF MELANOMA USING FEATURES EXTRACTED FROM THE SEGMENTED REGIONS

Nabin K. Mishra[a], Randy H. Moss[a], Bijaya Shrestha[a], William V. Stoecker[b]

[a]Department of Electrical and Computer Engineering, Missouri University of Science and Technology (S&T), Rolla, MO, 65409, USA

[b]Stoecker & Associates, Rolla, MO, 65401, USA

ABSTRACT

In this paper classification of melanoma is performed based on features extracted from atypical pigment network (APN) in dermoscopy images of skin lesions. Here APN includes different types of atypical network aberrations including branch streaks, radial streaming, pseudopods, and other irregular wide and/or dark network areas. First, automatic segmentation of APN based on the variance in the red plane is performed in the lesion area. Various features involving morphology, color and texture of the segmented APN region are extracted. Some features related to morphology of the lesion are also calculated. These features are used to build a prediction model based on logistic regression for the classification of melanoma using a training set of 837 dermoscopy images taken recently from private practice clinics, to most closely resemble real-world data and also have real-world difficulty, with a melanoma to benign ratio of 1.35. The model so obtained is then used on a disjoint test set of size 804 dermoscopy images which are similar in difficulty to the training set, with a similar melanoma to benign ratio.

At a sensitivity of 97.2% for the training set, the model provided a sensitivity of 80.42%

for the test set.

1. INTRODUCTION

Skin cancer is a very common type of cancer among both sexes in the United

States. There are different types of skin cancer and melanoma is one which is considered

to be the deadliest as it is responsible for the most skin cancer deaths. In the year 2014, an

estimated 76,100 new cases of invasive malignant melanomas will be diagnosed in the

United States [2]. And, about 9,710 people are expected to die of melanoma in the same

year [2]. Failure to diagnose melanoma in its earlier stage may allow it to be lethal. Early

detection of melanoma, at the in-situ stage, results in no change in life expectancy [3].

Thus, early detection of melanoma is significantly important for reducing deaths caused

by melanoma. Over a billion dollars per year is spent on biopsying lesions that turn out to

be benign, and even then cases of melanoma are missed by domain experts [4].

In this research, melanoma detection is performed based on features extracted

from Atypical Pigment Network (APN) areas within the boundary of a skin lesion in a

dermoscopy image. Dermoscopy imaging has been reported to be a very useful tool in the

early recognition of melanoma [5-8]. It has been shown from various studies that

dermoscopy increases the diagnostic accuracy over clinical visual inspection in the hands

of experienced physicians [9-11]. Hence automatic analysis of dermoscopic images using

image processing methods to segment important melanoma features has been a popular

area of research in recent years. An APN is one among many such features which is often

found in the early stage of melanoma, yielding an odds ratio of 9.0 compared to benign

lesions [12]. Due to this reason it is considered to be a very critical feature in early detection of melanoma.

APN regions are brown, black or gray meshes or thick lines in dermoscopy images [13]. They are branched, broken-up, thickened and asymmetrical structure found in melanocytic skin lesions [9,12,14]. This paper follows the consensus conference nomenclature [12] and Fleming et al. [15], and include branch streaks, radial streaming, pseudopods, and other darkened or thickened network areas in the definition of APN. There have been several studies in segmentation of APN but not many have addressed the importance of APN in melanoma classification [15-19]. Fleming et al. [15] present techniques for extraction and measurement of important characteristics of the network including thickness, variability of thickness of network lines, the size and variability of network holes; and the presence or absence of radial streaming and pseudopods close to network periphery. Fischer et al. [16] describes a technique for enhancement of network pattern but does not accomplish network segmentation. Anantha et al. [17] presents a global non-extractive texture analysis of two methods for determination of pigment network; one based on the neighboring gray-level dependence matrix (NGLDM) and the other using the lattice aperture waveform set (LAWS). Betta et al. [18] describes a method of detecting pigment network by using a combination of spectral and structural technique. Sadeghi et al. [19] proposes a graph-based method of detecting pigment network, based on the fact that the edges of pigment network structures form cyclic graphs which can be automatically detected and analyzed.

This research involves the segmentation of APN regions, feature extraction from the segmented regions and finally classification of melanoma based on extracted features.

APN segmentation is based on a simple concept of variance in the red plane being important for the detection of pigment network in a dermoscopy image [20]. In addition, few morphological features related to the skin lesion and clinical features are also used for melanoma and benign lesion classification.

Figure 1 shows a simple block diagram of the work presented in this research. The input to the system is a simple RGB dermoscopy image of a skin lesion and the final outcome is to be able to decide whether the image is of a melanoma or a benign lesion.
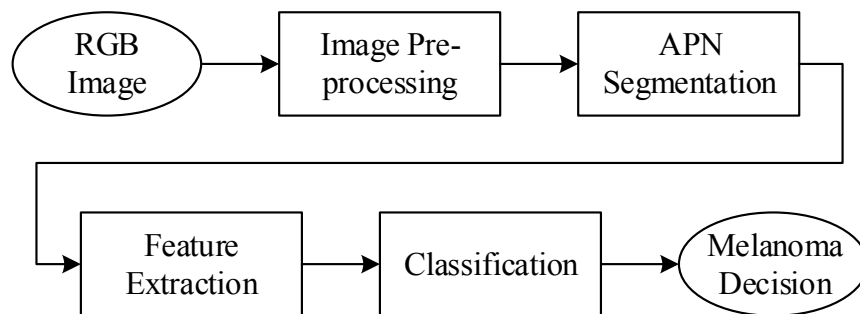
Figure 1. Block diagram showing classification of melanoma using APN segmentation.

The rest of the paper is organized as follows. Section 2 describes the APN segmentation process. Section 3 explains the features extracted from the APN segmented region. Section 4 gives the classification methodology along with the explanation of image data. Section 5 presents the results from the classifier. Finally. Section 6 discusses the conclusion.

2. APN SEGMENTATION

Segmentation of APN starts with a pre-processing of the dermoscopy image. The image is divided into non-overlapping blocks of size 16 by 16. A previously developed automatically generated hair mask is used to identify blocks which incorporate any part of hair mask. These blocks are excluded from any further analysis and only those blocks which are within the lesion border and do not contain any hair are used for segmentation purposes. Similarly, manually marked bubble masks are also used to mask out bubble areas inside the lesion region before APN segmentation algorithm is implemented.

Preliminary analysis was performed on some dermoscopy images with manually segmented APN area. This analysis showed variance in the red plane as a major factor in segmentation of APN. The importance of red variance in images for melanoma detection was first described by Umbaugh et al. [20]. Analysis of APN areas showed that all areas ranked above the sum of mean and one standard deviation of block red variance implies APN on adaptive block variance ranking. The 16 by 16 block size is also motivated by Umbaugh's block size of 8x8 for his 500 X 480 images, providing the optimal level of resolution for discrimination of melanoma from benign images. Figure 2 shows a dermoscopy skin lesion with manually marked APN region. Figure 3 shows two-dimensional and three-dimensional contour plots of red plane variance, for the same image, indicating the target APN region in the skin lesion, denoted by red contours. It should also be noted that artifacts like bubbles and hairs which are outside the lesion borders, in this case, also have high red variance. Hence, artifacts removal is an essential step in APN segmentation.
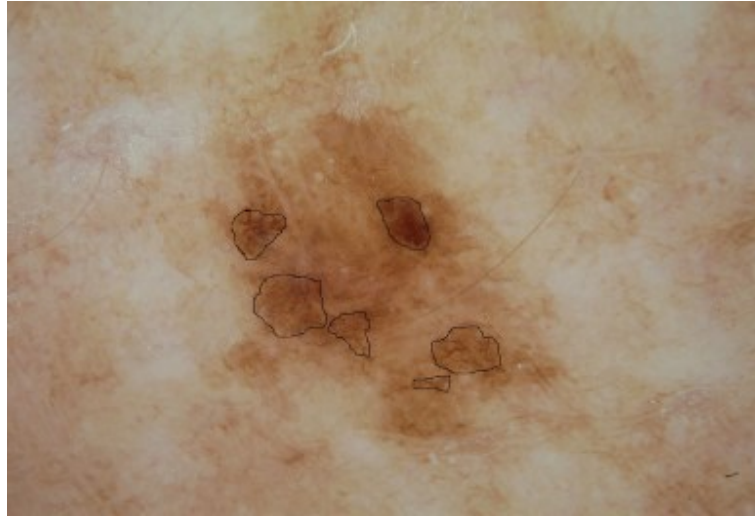
Figure 2. Dermoscopy lesion image with APN region marked manually.
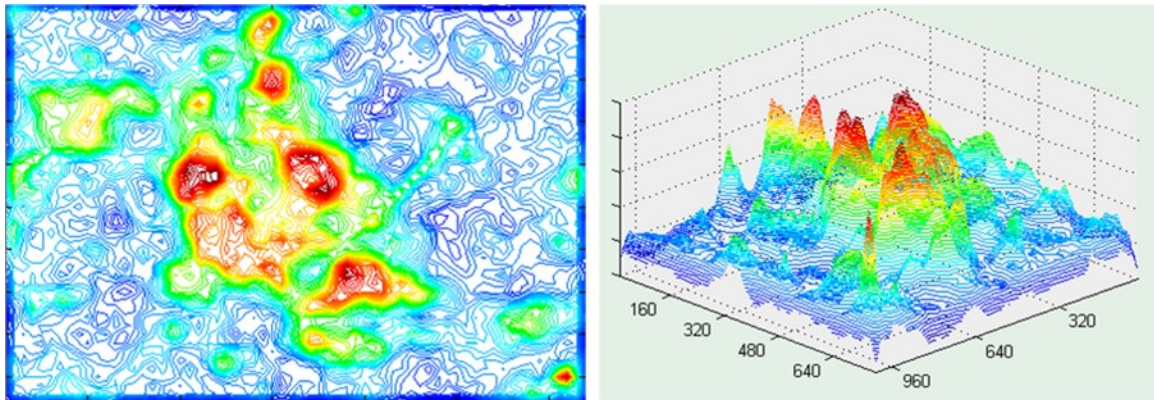
Figure 3. Two-dimensional and three-dimensional contour plot of red plane variance.

Red plane variance is calculated in a block size of 16 by 16 for the blocks that are within the lesion boundary and not part of the hair mask. Eq. (1) shows the mathematical formula used to calculate variance in the red plane for each non-overlapping block. The

variance value is stored in each pixel location of the block after calculation. Value of N in Eq. (1) is 256.

$$varR(x,y) = \frac{1}{N-1} \sum_{i=1}^{\sqrt{N}} \sum_{j=1}^{\sqrt{N}} \left(Ir\left(\sqrt{N} * (x-1) + i, \sqrt{N} * (y-1) + j\right) \right.$$

$$\left. - \frac{1}{N} \sum_{u=1}^{\sqrt{N}} \sum_{v=1}^{\sqrt{N}} Ir\left(\sqrt{N} * (x-1) + u, \sqrt{N} * (y-1) + v\right) \right)^{2} \qquad (1)$$

where $varR(x,y)$ is the red plane variance in a square block containing N pixels; $x = 1 \dots 1024/\sqrt{N}$ and $y = 1 \dots 768/\sqrt{N}$ for an image of size 1024x768 with x being the vertical coordinate and y being the horizontal coordinate; and Ir is the red plane of the dermoscopy image.

A threshold value is calculated, as shown in Eq. (2), from the overall mean and standard deviation of the variance calculated in Eq. (1). An intermediate APN mask is obtained by applying the APN threshold, calculated using Eq. (2), over the blocks used for variance calculation. This is shown in Eq. (3). The APN mask provided by Eqs. (2) and (3) include all relevant APN areas, as shown in Figure 4(a) and 4(f).

$$APN_{threshold} = mean(varR) + std(varR) \qquad (2)$$

$$A_{interm}(x,y) = \begin{cases} 1, & if\ varR(x,y) > APN_{threshold} \\ 0, & otherwise \end{cases} \qquad (3)$$

In order to remove some of the false positive blocks, which contain blue-gray granular areas, a green-to-blue ratio is calculated as shown in Eq. (4), where $avgG(x,y)$ and $avgB(x,y)$ represent the block by block average of the green plane and the blue plane of the lesion dermoscopy image, respectively. Any part of the intermediate APN

mask having a green-to-blue ratio of less than 1.1 is rejected to obtain the final APN

mask as shown in Eq. (5)

$$GB_{ratio}(x,y) = \frac{avgG(x,y)}{avgB(x,y)} \tag{4}$$

$$A(x,y) = \begin{cases} 1, & if\ GB_{ratio}(x,y) \geq 1.1\ and\ A_{interm}(x,y) = 1 \\ 0, & otherwise \end{cases} \tag{5}$$
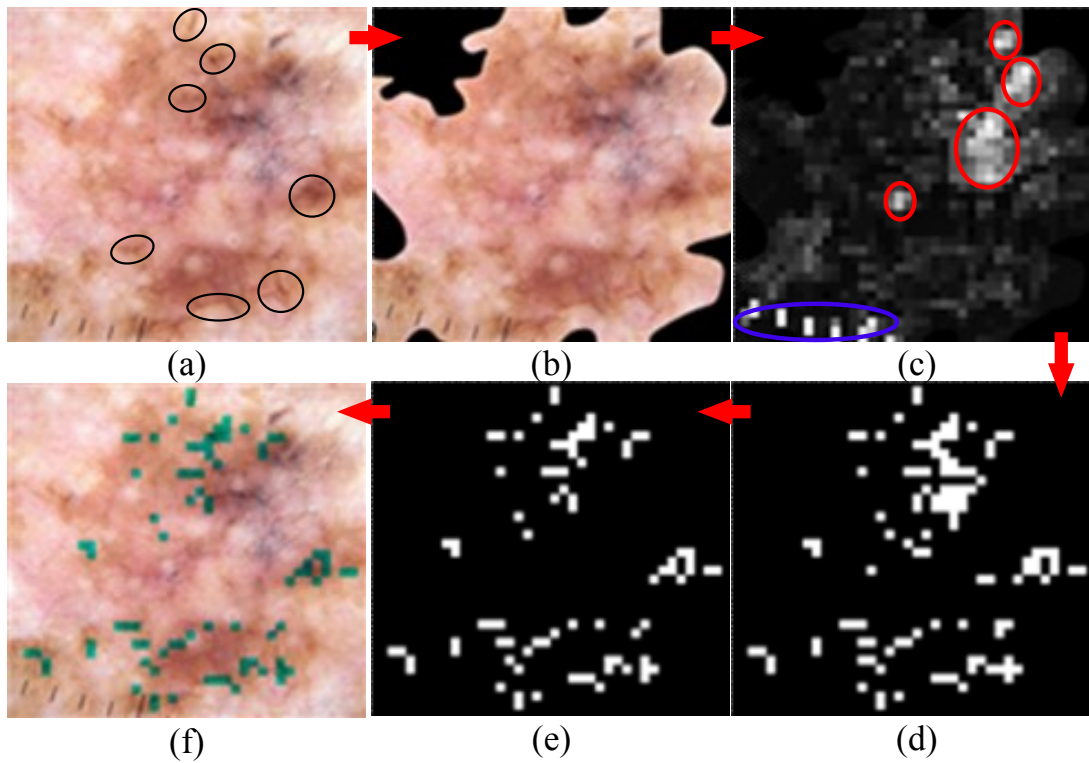
Figure 4. APN segmentation in a melanoma *in situ* image. (a) Original image, (APN circled) (b) lesion mask, (c) relative red plane variance, highest for granularity (red circles) and ruler markings (blue oval), (d) red variance mask after threshold, (e) mask after threshold for green-to-blue ratio applied, (f) final overlaid APN mask [21].

Figure 4 demonstrates the steps of APN segmentation starting from the target

APN region in Figure 4(a) and finally obtaining an APN overlay in Figure 4(f).

Figure 5 shows two sample dermoscopy images with their respective APN overlays.
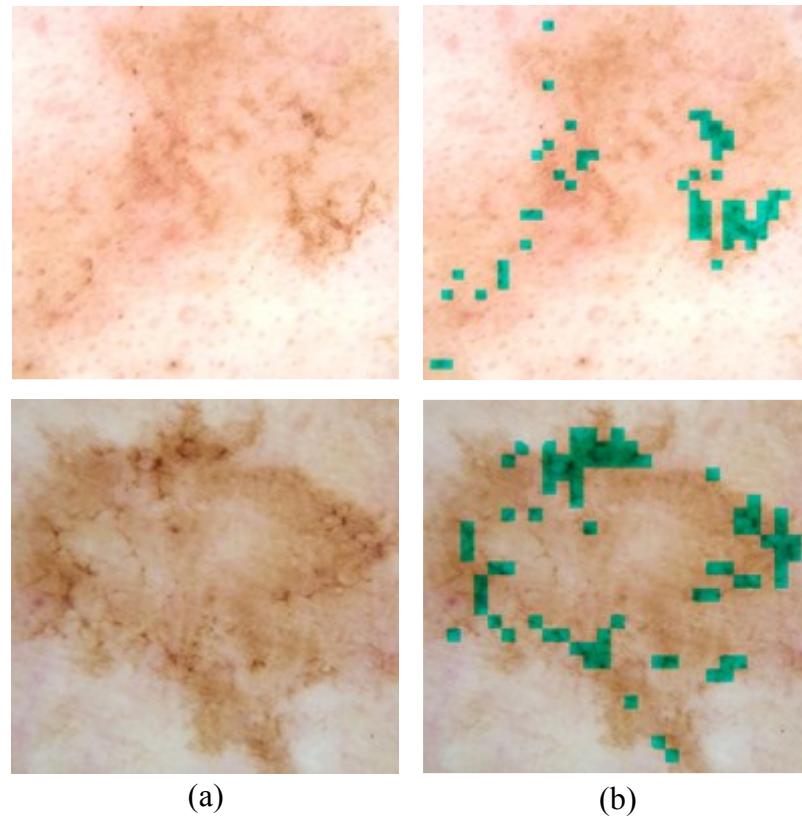
Figure 5. Samples of dermoscopic lesion with APN. (a) Lesion image, (b) APN overlay on lesion.

3. FEATURE EXTRACTION

A total of fifty-one different features are extracted for the classification of melanoma. Twelve of these features are morphological features related to the APN region and the lesion segment. Eleven of these features are texture features. The other twenty-eight features are color-related features for the APN region in the lesion.

3.1. MORPHOLOGICAL FEATURES

Morphological features are features related to the morphology of the lesion or of the segmented APN region or of a combination of both. The list of morphological features used in this research is shown in Table 1. In Table 1, R and C represent total number of rows and columns, respectively, of the dermoscopy image. $B(r, c)$ represents binary lesion mask where inside lesion area is represented by 1 and outside lesion area is represented by 0. $A(r, c)$ is the binary APN mask where 1 represents the APN region and 0 represents the non-APN region. In Table 1, APN block is defined as a 16 by 16 binary block representing APN region, and APN blob is defined as a group of one or more APN blocks connected together by 8-connetivity.

The centroid of a binary object with n number of pixels is given by,

$$X_c = \frac{1}{n} \sum_{i=1}^{n} x_i \tag{6}$$

$$Y_c = \frac{1}{n} \sum_{i=1}^{n} y_i \tag{7}$$

where x_i and y_i are the x and the y coordinates of pixels in the binary object.

Table 1. List of morphological features.

Feature #	Mathematical Formula	Feature Description
M1	$$Lesion_{area} = \sum_{r=1}^{R}\sum_{c=1}^{C} B(r,c)$$	Lesion area
M2	$$APN_{area} = \sum_{r=1}^{R}\sum_{c=1}^{C} A(r,c)$$	APN area
M3	$$\frac{APN_{area}}{Lesion_{area}}$$	Ratio of APN area to lesion area
M4	$$\frac{\# \, of \, APN \, blobs(8\_connected)}{Lesion_{area}}$$	Ratio of number of APN blocks to lesion area
M5	$$\frac{\# \, of \, APN \, blocks}{\# \, of \, APN \, blobs(8\_connected)}$$	Ratio of number of APN blocks to number of APN blobs (8-connected)
M6	$$D_c = \sqrt{(x_{c,APN} - x_{c,lb})^2 + (y_{c,APN} - y_{c,lb})^2}$$	Centroid distance between APN mask centroid $(x_{c,APN}, y_{c,APN})$ and lesion border mask centroid $(x_{c,lb}, y_{c,lb})$; centroid calculation is described in text below
M7	$$D_{c,LesNorm} = \frac{D_c}{\sqrt{Lesion_{area}}}$$	Lesion normalized centroid distance
M8	$$Lesion_{perimeter}$$	Total number of the outermost pixels of the lesion
M9	$$\frac{Lesion_{area}}{Image_{area}}$$	Ratio of lesion area to image area
M10	$$D_{c,APNnorm} = \frac{D_c}{\sqrt{APN_{area}}}$$	APN normalized centroid distance
M11	$$\frac{Lesion_{perimeter}}{\sqrt{Lesion_{area}}}$$	Ration of lesion perimeter to square root of lesion area
M12	$$\frac{Lesion_{perimeter}}{\sqrt{APN_{area}}}$$	Ration of lesion perimeter to square root of APN area

3.2. MEDIAN SPLIT FEATURES

Median split is a method of clustering of an image by color into more than one segments using the histogram of the image [22-25]. The median split features are considered only for the lesion area, hence the border mask is used to segment the lesion. Initially all pixels in the lesion area are considered to be in a single color bin with three dimensions, R, G and B. The dimension with the largest range is then split at the median, so there are an equal number of pixels in the two resulting bins. Each iteration then considers the ranges of the colors of each of the bins and splits the bin with the largest range into two bins with equal pixel populations. The bin with the highest range in any color axis is chosen for the subsequent split. Within the chosen bin, the split is performed along the color axis with this highest range. In this research, this is performed three times resulting in a segmentation into four color regions. Each region is then represented by its average color. Figure 6 illustrates median split obtained from original RGB image. It should be noted that lesion mask was applied on the RGB image before implementing the median split algorithm.

(a)   (b)   (c)
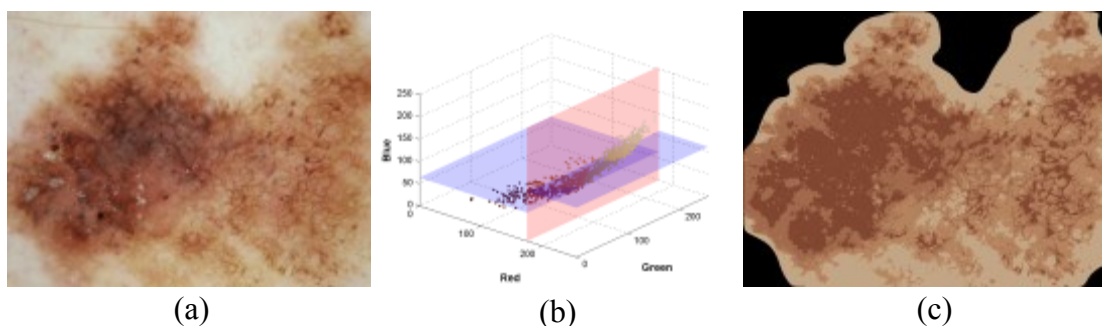
Figure 6. Median split image obtained for a lesion. (a) Original lesion, (b) Histogram in 3-D space, (c) Median split image.

The area of APN segments lying in each color region of a median split image is used as a feature in this research for melanoma identification. These features are normalized by total APN area and the total lesion area as shown in Eq. (8) and Eq. (9).

$$MS_{i,APNnorm} = \frac{\sum_{r=1}^{R}\sum_{c=1}^{C}\big(MS_i(r,c) * A(r,c)\big)}{\sum_{r=1}^{R}\sum_{c=1}^{C}A(r,c)} \tag{8}$$

$$MS_{i,LesionNorm} = \frac{\sum_{r=1}^{R}\sum_{c=1}^{C}\big(MS_i(r,c) * A(r,c)\big)}{\sum_{r=1}^{R}\sum_{c=1}^{C}B(r,c)} \tag{9}$$

where i = 1 … 4 represents the 4 different colors of the median split image; i = 1 correspond to the darkest segment and i = 4 correspond to the lightest segment. $MS_i(r,c)$ is the binary median split mask representing the ith color. $A(r,c)$ represents the binary APN mask and $B(r,c)$ represents the binary lesion border mask.

3.3. SALIENT POINT FEATURES

Motivation of finding salient points came from the fact that atypical pigments are critical in finding melanoma. Salient points are detected using Steger's method of line detection [26]. The best results in terms of melanoma discrimination were obtained from the intensity plane *(R+G+B)/3* [27]. The choice of sigma in Gaussian filter for the purpose of blurring also affected the outcome and its optimal value was 1.02 [27]. Hence, in this research, salient points obtained from the intensity plane blurred using a Gaussian filter at a sigma value of 1.02 were used to extract features. Figure 7 shows a sample of a lesion image and its salient point mask.
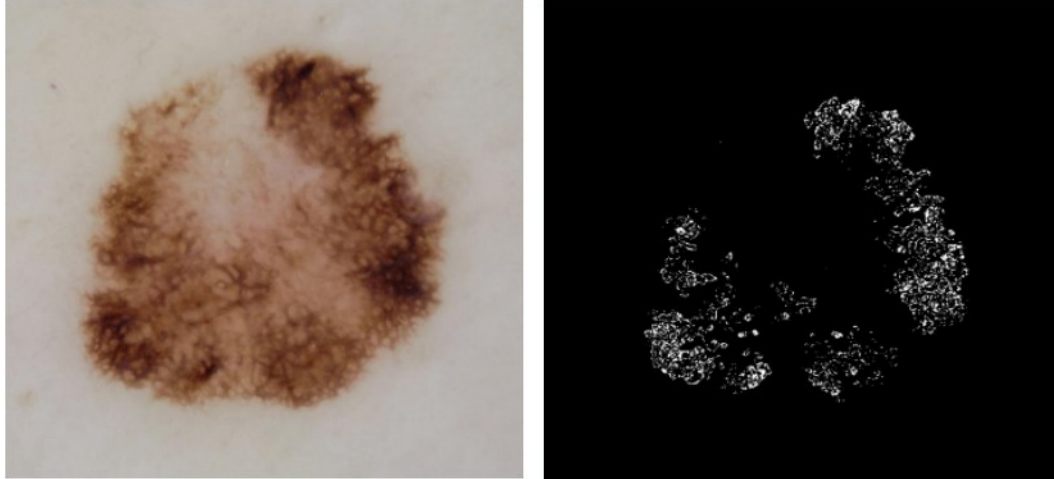
Figure 7. A lesion image and its salient point mask.

Salient point features are summarized in Table 2. In Table 2, $S(r,c)$ represent the salient point mask with a value of 1 representing a salient point and 0 otherwise. Similary, $A(r,c)$ and $B(r,c)$ represents the APN and the lesion border masks, respectively, which are also binary where 1 represents the corresponding region and 0 otherwise.

Table 2: List of salient point features.

Feature #	Mathematical Formula	Feature Description
S1	$\sum_{r=1}^{R}\sum_{c=1}^{C}(S(r,c) * A(r,c))$	Salient point count in APN region
S2	$\dfrac{\sum_{r=1}^{R}\sum_{c=1}^{C}(S(r,c) * A(r,c))}{\sum_{r=1}^{R}\sum_{c=1}^{C} A(r,c)}$	Salient point count in APN region normalized by APN area
S3	$\dfrac{\sum_{r=1}^{R}\sum_{c=1}^{C}(S(r,c) * A(r,c))}{\sum_{r=1}^{R}\sum_{c=1}^{C} B(r,c)}$	Salient point count in APN region normalized by lesion area
S4	$\sum_{r=1}^{R}\sum_{c=1}^{C}(S(r,c) * B(r,c))$	Salient point count in lesion area
S5	$\dfrac{\sum_{r=1}^{R}\sum_{c=1}^{C}(S(r,c) * B(r,c))}{\sum_{r=1}^{R}\sum_{c=1}^{C} B(r,c)}$	Salient point count in lesion area normalized by lesion area

3.4. TEXTURE FEATURES

First-order texture features of the APN regions, calculated using characteristics of the gray-level intensity histogram, are also used for identifying melanoma. Six histogram characteristics [28] are chosen as texture features in this research as shown in Table 3. These features are calculated only for the APN region using the APN mask and the grayscale image. The RGB lesion image is converted to a grayscale image by using Eq. (10). *R, G,* and *B* are the intensity values of the red, the green and the blue planes, respectively.

$$I_{gray} = 0.2989 * R + 0.5870 * G + 0.1140 * B \tag{10}$$

Table 3: List of texture features for APN region.

Feature #	Mathematical Formula	Feature Description
T1	$\sum_{level=1}^{N} I_{level} * p_{level}$	Histogram mean; it measures average brightness; where I_{level} is the intensity level in the histogram and p_{level} is the probability of that intensity level
T2	$\sum_{level=1}^{N} (I_{level} - H_{mean})^2 * p_{level}$	Histogram variance; it measures average contrast; where H_{mean} is the histogram mean (T1)
T3	$1 - \dfrac{1}{1 + H_{var}^2}$	Smoothness index measures the relative smoothness of the region; where H_{var} is the histogram variance (T2)
T4	$\sum_{level=1}^{N} (I_{level} - H_{mean})^3 * p_{level}$	Skewness index measures the skewness of the histogram; a value of 0 represents a symmetric histogram while a positive or negative value indicates a skewed histogram
T5	$\sum_{level=1}^{N} p_{level}^2$	Uniformity index measures uniformity and has a maximum value when all intensity levels are equal
T6	$\sum_{level=1}^{N} p_{level} * \log_2(p_{level})$	Entropy measures the information content of a message and its higher value indicates greater information

3.5. COLOR FEATURES

The average color intensity of the red, green and blue color planes in the APN regions and their standard deviation as shown in Table 4 are used as color features in the detection of melanoma using APN. In Table 4, AC1, ..., AC6 represents color features for APN region inside the lesion border. These features are also calculated for the non-APN region inside the lesion border which are represented by nAC1, …, nAC6. In Table 4, N represents total number of pixels in APN region and i is used to index pixels in that region. Similar notation also applies to non-APN region feature calculation.

Table 4. List of RGB color features for APN region inside lesion.

Feature #	Mathematical Formula	Feature Description
AC1	$\bar{R} = \dfrac{1}{N}\displaystyle\sum_{i=1}^{N} I_{red}(i)$	Average intensity of red color in APN region; I_{red} is the red plane intensity value
AC2	$\bar{G} = \dfrac{1}{N}\displaystyle\sum_{i=1}^{N} I_{green}(i)$	Average intensity of green color in APN region; I_{green} is the green plane intensity value
AC3	$\bar{B} = \dfrac{1}{N}\displaystyle\sum_{i=1}^{N} I_{blue}(i)$	Average intensity of blue color in APN region; I_{blue} is the blue plane intensity value
AC4	$stdR = \sqrt{\dfrac{1}{N-1}\displaystyle\sum_{i=1}^{N}(I_{red}(i) - \bar{R})^2}$	Standard deviation of intensity of red color in APN region
AC5	$stdG = \sqrt{\dfrac{1}{N-1}\displaystyle\sum_{i=1}^{N}(I_{green}(i) - \bar{G})^2}$	Standard deviation of intensity of green color in APN region
AC6	$stdB = \sqrt{\dfrac{1}{N-1}\displaystyle\sum_{i=1}^{N}(I_{blue}(i) - \bar{B})^2}$	Standard deviation of intensity of blue color in APN region

Color features are also calculated using hue plane data for the APN and the non-APN regions, inside the lesion. The RGB image is hence converted into HSV (hue, saturation and value) planes. Since hue is a circular quantity different measures are used to calculate hue related features. These features are summarized in Table 5 [29-32].

In order to calculate these features, some additional quantities are calculated. Hue, a circular quantity, is converted into complex number representation as in Eq. (11).

$$H_z = exp\left(i * H * \frac{pi}{180}\right) \qquad (11)$$

Sample first moment or the mean resultant vector is then calculated using Eq. (12). In Eq.

(12) N represents the total number of pixels in the region used for calculating features.

$$\rho_1 = \frac{1}{N} \sum_{j=1}^{N} H_z \tag{12}$$

The length of the mean resultant vector for the first moment is as shown in Eq. (13).

$$R_1 = abs(\rho_1) \tag{13}$$

The sample second moment is calculated using Eq. (14) and the value is used to calculate

the length of the second moment as in Eq. (15).

$$\rho_2 = \frac{1}{N} \sum_{j=1}^{N} H_z^2 \tag{14}$$

$$R_2 = abs(\rho_2) \tag{15}$$

Similarly, as shown in Table 5, hue plane features are calculated for the non APN region

inside the lesion. These features are represented by nAH1, …, nAH4.

Table 5. List of hue plane features for APN region inside the lesion.

Feature #	Mathematical Formula	Feature Description
AH1	$H_{mean} = angle(\rho_1) * \dfrac{180}{pi}$	Mean hue
AH2	$H_{var} = 1 - R_1$	Hue variance
AH3	$H_{std} = \sqrt{-2 * \ln(R_1)}$	Hue standard deviation
AH4	$H_{disp} = \dfrac{1 - R_2}{2 * R_1^2}$	Hue dispersion

4. DATA DESCRIPTION

Skin lesion images for the experiment are acquired from four private practice clinic locations in the USA. These are contact nonpolarized dermoscopy images taken using similar devices under similar lighting conditions and at the same magnification level. All images are 1024 by 768 resolution full color images in jpeg format.

This image data is divided into two disjoint sets: a training set and a test set. The training set consists of 837 lesion images with 184 melanomas and 653 benign lesions. The test set consists of 804 lesion images with 189 melanomas and 615 benign lesions. Lesion border masks for each of these images used in this research are manually acquired from the domain expert. An automatically generated hair mask is used in the pre-processing.

5. RESULTS AND DISCUSSION

A total of fifty one different features described in Section 3 (12 morphological features, 8 median split features, 5 salient point features, 6 texture features, 12 RGB color features and 8 hue color features) are used in a logistic regression based classifier with an objective to identify melanoma automatically. Figure 8 shows the receiver operating characteristic (ROC) curve for the APN classifier model. The area under the ROC curve (AUC) for the model is 0.902.
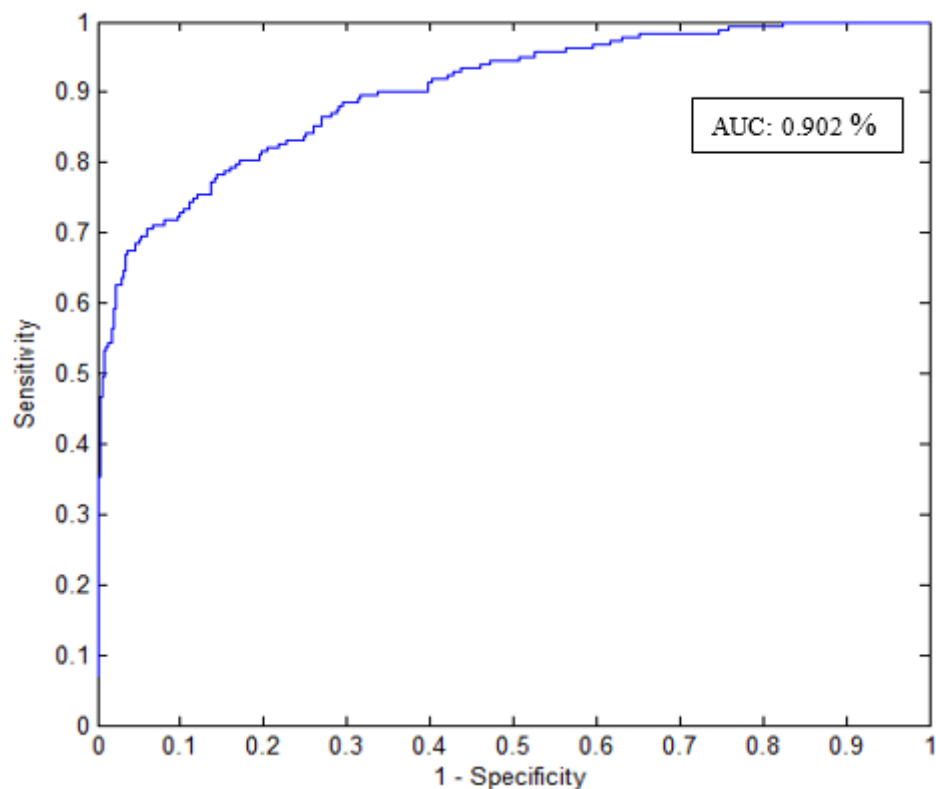
Figure 8. ROC curve for melanoma classification using APN features.

The maximum accuracy of the model at an AUC of 0.902 was achieved to be 84.9%, meaning the model was capable of correctly classifying melanoma and benign lesions approximately around 85% of the time. The objective here is to maximize the sensitivity such that chances of missing the detection of melanoma are very small. As a result a threshold was chosen such that the sensitivity is 97.2% for the training set; at this point specificity was calculated to be 41.35% for the training set. With the same threshold, sensitivity was 80.42% while the specificity was 33.01% for the test set.

Table 6 shows the top ten features selected in the model along with their chi-square score.

Table 6: Top ten features in the model with their chi-square score.

S.N.	Feature Description	Feature	Chi-Square Score
1	Lesion perimeter	M8	105.9414
2	Hue standard deviation in non APN region	nAH3	37.151
3	Ratio of lesion perimeter to square root of lesion area	M11	34.6872
4	APN normalized lowest intensity median split area in APN	MS1	9.8186
5	Red plane standard deviation in APN area	AC4	7.5416
6	Green plane standard deviation in non APN area	nAC5	14.5247
7	Mean hue in APN area	AH1	8.5233
8	Blue plane standard deviation in non APN area	nAC6	15.0423
9	Interaction feature	nAH3*nAC6	7.2715
10	Interaction feature	M8*nAH3	11.6056

Figure 9 shows two samples of 2 mm melanoma dermoscopy lesion images along with their APN overlay. These two samples were successfully identified as melanoma using the model based on APN features presented in this paper.
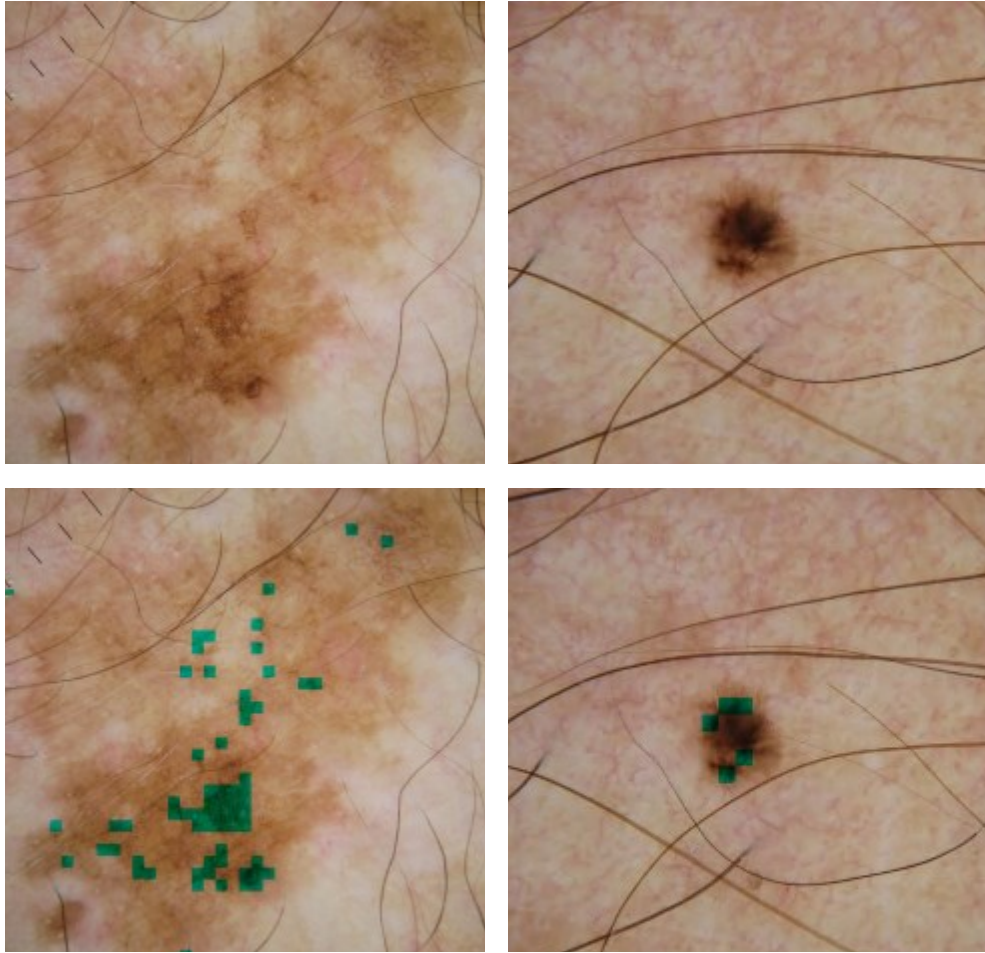
Figure 9. Samples of 2mm melanoma detected successfully using APN model.

6. CONCLUSION

In this research, segmentation of the APN region in a skin lesion is performed based on the idea that the red plane variance is significant for finding the APN region. A variety of features extracted from the APN region are then used to explore the classification of melanoma and benign lesions. A logistic regression based classifier model is designed to perform discrimination of melanoma from benign lesions. This model achieved an overall accuracy of almost 85% on a large real world data set. With

the objective of achieving high sensitivity, the model threshold can be modified to get sensitivity of 97.2% with a specificity of 41.35% for the training set whereas a sensitivity of 80.42% and a specificity of 33.01% result for the test set at the same threshold. The statistical results based on APN features from this research demonstrate that APN is a critical feature in identifying melanoma and these features in combination with other melanoma image features could further improve the accuracy in identifying melanoma from the dermoscopic image.

ACKNOWLEDGMENTS

REFERENCES

1. Stricklin, Sherea M., William V. Stoecker, Joseph M. Malters, Rhett Drugge, Margaret Oliviero, Harold S. Rabinovitz, and Lindall A. Perry. "Melanoma in situ in a private practice setting 2005 through 2009: location, lesion size, lack of concern." *Journal of the American Academy of Dermatology* 67, no. 3 (2012): e105-e109.

2. Siegel, Rebecca, Jiemin Ma, Zhaohui Zou, and Ahmedin Jemal. "Cancer statistics, 2014." *CA: A Cancer Journal for Clinicians* 64, no. 1 (2014): 9-29.

3. Mocellin, Simone, and Donato Nitti. "Cutaneous melanoma in situ: translational evidence from a large population-based study." *The Oncologist* 16, no. 6 (2011): 896-903.

4. "The Cost of Cancer." National Cancer Institute at the National Institutes of Health. 2011. *http://www.cancer.gov/aboutnci/servingpeople/understandingburden/costof cancer.*

5. Pehamberger, Hubert, Michael Binder, Andreas Steiner, and Klaus Wolff. "In vivo epiluminescence microscopy: improvement of early diagnosis of melanoma." *Journal of Investigative Dermatology* 100 (1993): 356S-362S.

6. Soyer, H. Peter, Giuseppe Argenziano, Sergio Chimenti, and Vincenzo Ruocco. "Dermoscopy of pigmented skin lesions." *European Journal of Dermatology* 11, no. 3 (2001): 270-7.

7. Soyer, H. Peter, Giuseppe Argenziano, Renato Talamini, and Sergio Chimenti. "Is dermoscopy useful for the diagnosis of melanoma?" *Archives of Dermatology* 137, no. 10 (2001): 1361-1363.

8. Stolz, Wilhelm, Otto Braun-Falco, Peter Bilek, Michael Landthaler, Walter HC Burgdorf, and Armand B. Cognetta, eds. *Color Atlas of Dermatoscopy*. Wiley-Blackwell, 2002.

9. Braun, Ralph P., Harold S. Rabinovitz, Margeret Oliviero, Alfred W. Kopf, and Jean H. Saurat. "Pattern analysis: a two-step procedure for the dermoscopic diagnosis of melanoma." *Clinics in Dermatology* 20, no. 3 (2002): 236-239.

10. Boldrick, Jennifer C., Christle J. Layton, Josephine Nguyen, and Susan M. Swetter. "Evaluation of digital dermoscopy in a pigmented lesion clinic: clinician versus computer assessment of malignancy risk." *Journal of the American Academy of Dermatology* 56, no. 3 (2007): 417-421.

11. Perrinaud, A., O. Gaide, L. E. French, J-H. Saurat, A. A. Marghoob, and R. P. Braun. "Can automated dermoscopy image analysis instruments provide added benefit for the dermatologist? A study comparing the results of three systems." *British Journal of Dermatology* 157, no. 5 (2007): 926-933.

12. Argenziano, Giuseppe, H. Peter Soyer, Sergio Chimenti, Renato Talamini, Rosamaria Corona, Francesco Sera, Michael Binder, Lorenzo Cerroni, Gaetano De Rosa, Gerardo Ferrara, Rainer Hofmann-Wellenhof, Michael Landthaler, Scott W. Menzies, Hubert Pehamberger, Domenico Piccolo, Harold S. Rabinovitz, Roman Schiffner, Stefania Staibano, Wilhelm Stolz, Igor Bartenjev, Andreas Blum, Ralph Braun, Horacio Cabo, Paolo Carli, Vincenzo De Giorgi, Matthew G. Fleming, James M. Grichnik, Caron M. Grin, Allan C. Halpern, Robert Johr, Brian Katz, Robert O. Kenet, MD, Harald Kittler, Jürgen Kreusch, Josep Malvehy, Giampiero Mazzocchetti, Margaret Oliviero, Fezal Özdemir, Ketty Peris, Roberto Perotti, Ana Perusquia, Maria Antonietta Pizzichetta, Susana Puig, Babar Rao, Pietro Rubegni, Toshiaki Saida, Massimiliano Scalvenzi, Stefania Seidenari, Ignazio Stanganelli, Masaru Tanaka, Karin Westerhoff, Ingrid H. Wolf, Otto Braun-Falco, Helmut Kerl, Takeji Nishikawa, Klaus Wolff, Alfred W. Kopf. "Dermoscopy of pigmented skin lesions: results of a consensus meeting via the Internet." *Journal of the American Academy of Dermatology* 48, no. 5 (2003): 679-693.

13. Argenziano, Giuseppe, Gabriella Fabbrocini, Paolo Carli, Vincenzo De Giorgi, Elena Sammarco, and Mario Delfino. "Epiluminescence microscopy for the diagnosis of doubtful melanocytic skin lesions: comparison of the ABCD rule of dermatoscopy and a new 7-point checklist based on pattern analysis." *Archives of Dermatology* 134, no. 12 (1998): 1563-1570.

14. Carli, P., E. Quercioli, S. Sestini, M. Stante, L. Ricci, G. Brunasso, and V. De Giorgi. "Pattern analysis, not simplified algorithms, is the most reliable method for teaching dermoscopy for melanoma diagnosis to residents in dermatology." *British Journal of Dermatology* 148, no. 5 (2003): 981-984.

15. Fleming, Matthew G., Carsten Steger, Jun Zhang, Jianbo Gao, Armand B. Cognetta, and Charles R Dyer. "Techniques for a structural analysis of dermatoscopic imagery." *Computerized Medical Imaging and Graphics* 22, no. 5 (1998): 375-389.

16. Fischer, Stefan, Philippe Schmid, and Joël Guillod. "Analysis of skin lesions with pigmented networks." In *Proceedings, International Conference on Image Processing, 1996*, vol. 1, pp. 323-326. IEEE, 1996.

17. Anantha, Murali, Randy H. Moss, and William V. Stoecker. "Detection of pigment network in dermatoscopy images using texture analysis." *Computerized Medical Imaging and Graphics* 28, no. 5 (2004): 225-234.

18. Betta, G., G. Di Leo, G. Fabbrocini, A. Paolillo, and P. Sommella. "Dermoscopic image-analysis system: estimation of atypical pigment network and atypical vascular pattern." In *IEEE International Workshop on Medical Measurement and Applications, 2006. MeMea 2006*, pp. 63-67. IEEE, 2006.

19. Sadeghi, Maryam, Majid Razmara, Tim K. Lee, and M. Stella Atkins. "A novel method for detection of pigment network in dermoscopic images using graphs." *Computerized Medical Imaging and Graphics* 35, no. 2 (2011): 137-143.

20. Kjoelen, Arve, Marc J. Thompson, Scott E. Umbaugh, Randy Hays Moss, and William V. Stoecker. "Performance of AI methods in detecting melanoma." *Engineering in Medicine and Biology Magazine, IEEE* 14, no. 4 (1995): 411-416.

21. Stoecker, William V., Nabin K. Mishra, Robert W. LeAnder, Ryan K. Rader, and R.J. Stanley, "Automatic detection of skin cancer - current status, path for the future." *In Proceedings of VISAPP* (1). (2013): 504-508.

22. Umbaugh, Scott E. *Digital Image Processing and Analysis: Human and Computer Vision Applications with CVIPtools*. CRC press, 2010.

23. Heckbert, Paul. "Color image quantization for frame buffer display." *SIGGRAPH Proceedings of the 9th annual conference on Computer Graphics and Interactive Techniques* (1982): 297-307.

24. Rosendahl, Cliff, Alan Cameron, Ian McColl, and David Wilkinson. "Dermatoscopy in routine practice: 'Chaos and clues'." *Australian Family Physician* 41, no. 7 (2012): 482.

25. Umbaugh, Scott E., Randy H. Moss, and William V. Stoecker. "Automatic color segmentation of images with application to detection of variegated coloring in skin tumors." *Engineering in Medicine and Biology Magazine, IEEE* 8, no. 4 (1989): 43-50.

26. Steger, Carsten. "Extracting lines using differential geometry and Gaussian smoothing." *International Archives of Photogrammetry and Remote Sensing* 31 (1996): 821-826.

27. Jella, Pavani. "Pigment network extraction and salient point analysis." M.S. Thesis in Electrical Engineering, University of Missouri, Rolla, MO, USA, 2004.

28. Gonzalez, Rafael C., and Richard E. Woods. *Digital Image Processing.* Prentice Hall, 2008.

29. Berens, Philipp. "CircStat: a MATLAB toolbox for circular statistics." *J Stat Softw* 31, no. 10 (2009): 4-8.

30. Mardia, Kanti V., and Peter E. Jupp. *Directional Statistics*. Vol. 494. John Wiley & Sons, 2009.

31. Fisher, Nicholas I. *Statistical Analysis of Circular Data*. Cambridge University Press, 1995.

32. Jammalamadaka, S. Rao, and Ambar Sengupta. *Topics in Circular Statistics*. Vol. 5. World Scientific, 2001.

III. AUTOMATED CLASSIFICATION OF MALIGNANT MELANOMA USING FUSION OF CLINICAL AND DERMOSCOPY FEATURES EXTRACTED FROM SKIN LESION IMAGES

Nabin K. Mishra[a], Randy H. Moss[a], Justin G. Cole[b], William V. Stoecker[b,c]

[a]Department of Electrical and Computer Engineering, Missouri University of Science and Technology (S&T), Rolla, MO, 65409, USA

[b]Stoecker & Associates, Rolla, MO, 65401, USA

[c]Department of Dermatology, University of Missouri School of Medicine, Columbia, MO, 65212, USA

ABSTRACT

Melanoma is the deadliest forms of skin cancer causing a large majority of skin cancer deaths. The number of deaths is only increasing every year. Since deaths caused by melanoma can be prevented if diagnosed early, its diagnosis in its early stage is extremely important. As such, automatic computer-based identification systems are one of the most efficient methods in early diagnosis of melanoma. This research presents an automated classification of melanoma and benign lesions using dermoscopy images. Various clinical and dermoscopy features are used in the classification method, which is based on logistic regression. Regions in a skin lesion image significant in identification of melanoma are segmented and then used to extract morphological, color and texture related features. These features are fused along with clinical features to build classifier models based on a training set that consists of real-world clinical dermoscopy images with a real-world melanoma to benign ratio. Models are built in a hierarchical manner

experimenting with different combination of features at different hierarchy levels. These models are then tested on a disjoint test set similar to the training set with a similar melanoma to benign ratio. Results obtained from these models are promising and provide a great amount of confidence in its practical implementation and future improvement.

1. INTRODUCTION

One of the most common types of cancer among both sexes in the United States is skin cancer. Among different types of skin cancer, malignant melanoma is considered to be the deadliest and is responsible for the most skin cancer deaths [1]. In 2014, an estimated 76,100 melanomas will be diagnosed and, about 9,710 people are expected to die of melanoma in the United States [1]. Failure to diagnose melanoma in its earlier stage may allow it to be lethal. Thus, early detection is critically important for reducing deaths caused by melanoma. However, decisions made by dermatologists for diagnosis of melanoma are highly subjective and they often depend on pathological tests which take time. Over a billion dollars per year is spent on biopsying lesions that turn out to be benign, and even then cases of melanoma are missed by domain experts [2]. Hence, professionals in the area seek computer-aided systems to assist with accurate diagnosis of melanoma and at the same time avoid performing numerous unnecessary biopsies. One reason for this is the enhancements in skin imaging technology and image processing techniques in recent decades. One purpose is to address and remove the subjectivity and ambiguity associated with the human decisions in the diagnosis process of melanoma. However, it is extensively accepted that any such computer-aided system and algorithm has to be highly accurate, in order to be implemented consistently in the diagnostic

process. In this research, clinical features and features extracted from dermoscopy images are used for automatic classification of melanoma.

In recent years, the dermoscopy imaging method has been very popular in skin cancer diagnosis. The importance of this imaging method in early diagnosis of melanoma has been widely reported in various studies [3-6]. Studies have also shown that dermoscopy increases the diagnostic accuracy over clinical visual inspection in hands of experienced physicians [7-9]. Hence dermoscopy images are very widely used in the automatic analysis of skin lesions for melanoma diagnosis.

There are multiple steps in automatic analysis of dermoscopy images for melanoma discrimination. Figure 1 shows the overall diagram of the system.
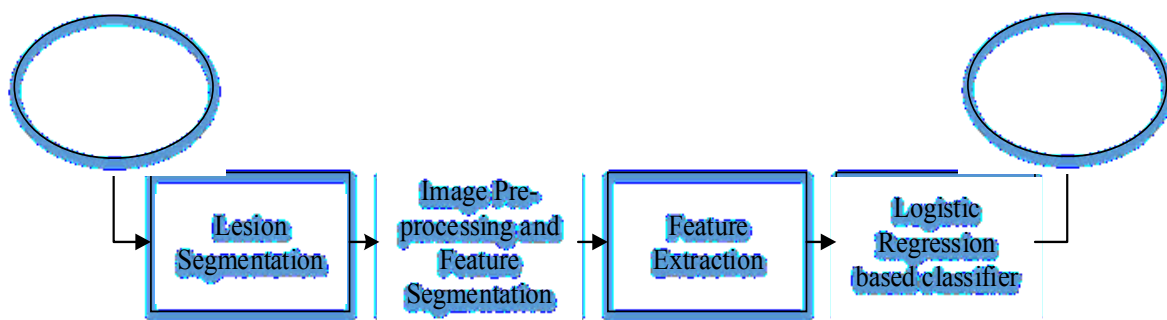
Figure 1. Overall block diagram of the automatic melanoma detection system.

The first step is the segmentation of the lesion from dermoscopy image. This step is followed by segmentation of local and global features. Local features are features that are present only in some parts of the lesion depending on lesion type and may either be characteristic of melanoma or benign lesions. Examples of these features are atypical pigment network (APN), white area, salient points and pink area. Segmentation of global

features is the division of entire lesion in terms of some global features like color. This research uses median split segmentation of the lesion as global feature segmentation. After this segmentation process, features are extracted based on morphology, color and texture statistics of the segmented regions. Clinical features related to lesion and patient are also collected to be used. The final step is the classification of melanoma and benign lesions based on the features generated in the previous step.

The subsequent sections of this report are organized as follows. Section 2 describes lesion segmentation and noise removal from the dermoscopy image. Section 3 explains in brief about feature sets used in this research. Section 4 describes image data set that is used in this research. Section 5 presents the classification process and the results achieved from the classification. Finally. Section 6 explains the conclusion of this research.

2. LESION SEGMENTATION AND ARTIFACT REMOVAL

Segmentation of the lesion area from the dermoscopy image is the first step in any analysis of local features that maybe significant for melanoma detection. In this research, manually drawn lesion borders are used in the analysis and segmentation of local melanoma features. These manual borders are drawn by experts in the field of dermatology. Figure 2 shows lesion segmentation using a manually obtained lesion border.
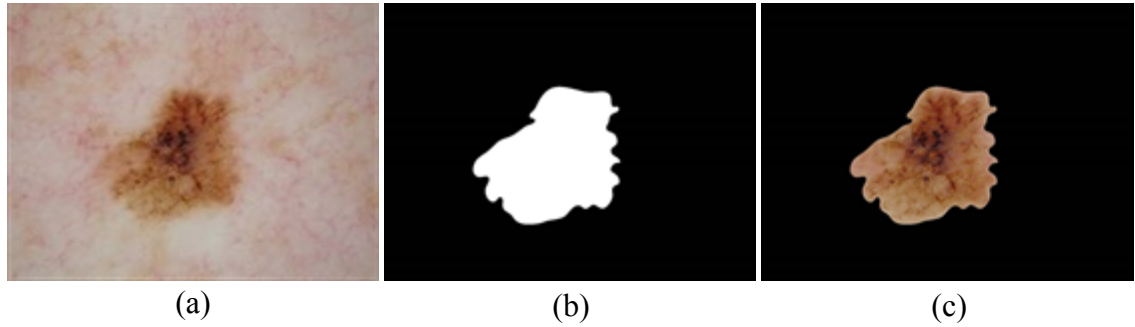
Figure 2. Lesion segmentation. (a) Dermoscopy lesion image, (b) Manually drawn lesion mask, (c) Segmented lesion area.

Hairs and bubbles in the dermoscopy liquid/gel act as artifacts in dermoscopy images and hence their proper masking is an essential pre-processing step for analysis of such images for accurate melanoma detection. An anisotropic diffusion based edge detection method is used to detect hair-like artifacts [10]. This method also detects edges of other useful lesion characteristics and hence a morphological noise removal technique is employed to remove non-hair segments. In regard to bubble artifacts, manually created bubble masks have been used in this research. The development of an automatic bubble mask is work in progress. Figure 3 shows the hair mask generation steps in brief.
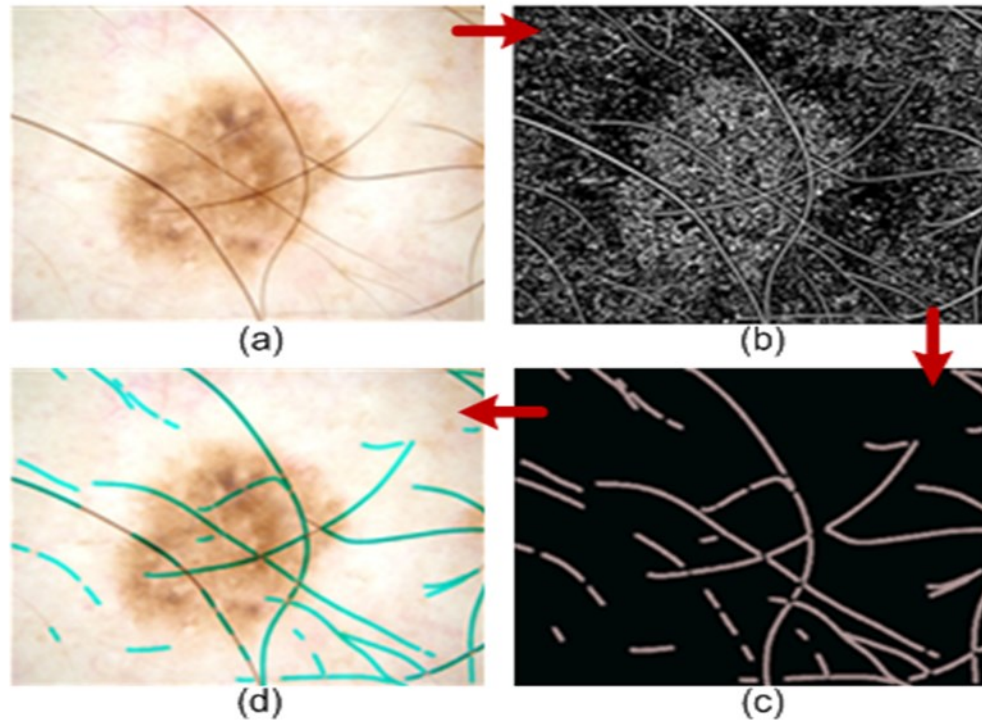
Figure 3. Segmentation of hair mask. (a) Original image, (b) Perona-Malik anisotropic diffusion [10], (c) Hair mask after noise removal, (d) Overlaid hair mask.

3. FEATURE DESCRIPTION

There are various factors that could determine the malignancy of a skin lesion. In this research, various different features are considered for discriminating melanoma from benign lesions. All these features are briefly described in this section.

3.1. CLINICAL FEATURES

Clinical features are features that are collected in clinic and may be related to patient's personal information and about the skin lesion. A list of clinical features used in this research are presented in Table 1.

Table 1. List of clinical features and their description.

Feature #	Feature Name	Feature Description
C1	Location of Patient	This is the geographic location of the patient. It is a binary feature and represents location either between 30°N latitude and 30°S latitude (in the equatorial region) or not.
C2	Age	Patient's age at the time of clinic visit.
C3	Gender	Gender of the patient: male or female.
C4	Quantized location	This represents the quantized location of lesion on the patient's body.
C5	Lesion size	This is the size of the largest dimension of the lesion in mm.
C6	Patient history	Any melanoma history in the patient; binary feature.
C7	Family history	Any melanoma history in the family of the patient; binary feature.
C8	Change	This is change observed in the skin lesion; binary feature.
C9	Patient concern	Concern shown by the patient due to the skin lesion; binary feature.

3.2. DERMOSCOPY FEATURES

Dermoscopy features are visual features that are local to the lesion area in dermoscopy images. Various dermoscopy features are used in this research. These feature regions are first segmented from the lesion area and then numerical features are extracted from the segmented regions. Each of the feature regions used in this research are described in brief.

3.2.1. Atypical Pigment Network (APN). APN regions are brown, black or gray meshes or thick lines in dermoscopy images [11]. It is a very critical feature for successful classification of melanoma. An atypical pigment network is often found in early stages of melanoma, yielding an odds ratio of 9.0 compared to benign lesions [12]. Using variance in the relative red plane, and a green-to-blue ratio threshold to remove false positives, APN can be found to classify melanoma. From preliminary analysis, it is observed that variance in the red plane is a major factor in segmentation of APN. Artifacts like hairs and bubbles also have similar red variance characteristic as APN, hence they are masked out using hair and bubble masks. Figure 4 shows a dermoscopy image along with the APN overlay.

(a)   (b)
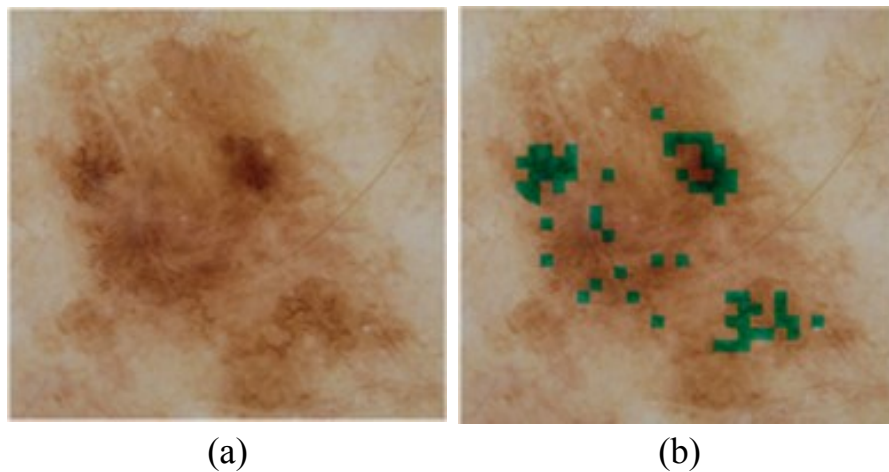
Figure 4. Sample dermoscopy image and APN overlay. (a) Original image, (b) APN overlay.

3.2.2. White Area. White areas are bright white spots generally considered to exist inside the lesion. However, they can also appear outside the apparent lesion borders, hence missed by automatic systems that analyze only the pigmented area. This research hypothesize that inclusion of white areas outside the apparent melanoma boundary in the analysis of a pigmented lesion may improve the accuracy of discrimination of melanoma from benign lesions [13-14]. Figure 5 shows the white area overlay inside and outside the lesion.
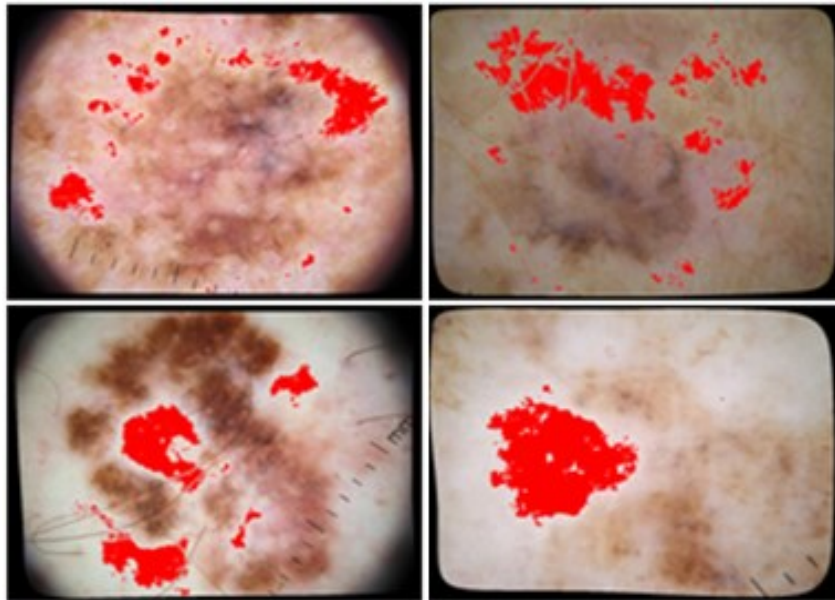
Figure 5. White area overlay inside and outside the lesion [13-15].

3.2.3. Median Split. A median split algorithm is used to cluster the lesion area by color into different segments [16-19]. This clustering method is based on the histogram of the lesion area. Initially all pixels are considered to be in a single color bin with three dimensions, R, G, and B. The dimension with the largest range is then split at the median, so there are an equal number of pixels in the two resulting bins. Each iteration then considers the ranges of the colors of each of the bins and splits the bin with the largest range into two bins with equal pixel populations. The bin with the highest range in any color axis is chosen for the subsequent split. Within the chosen bin, the split is performed along the color axis with the highest range. This is performed three times resulting in a segmentation into four color regions. Each region is then represented by its average color. A number of color-based and morphological features are generated based on each region of the segmented image [20]. Figure 6 shows the process of splitting the plane with highest range by displaying the histogram of the image.

(a) (b) (c)
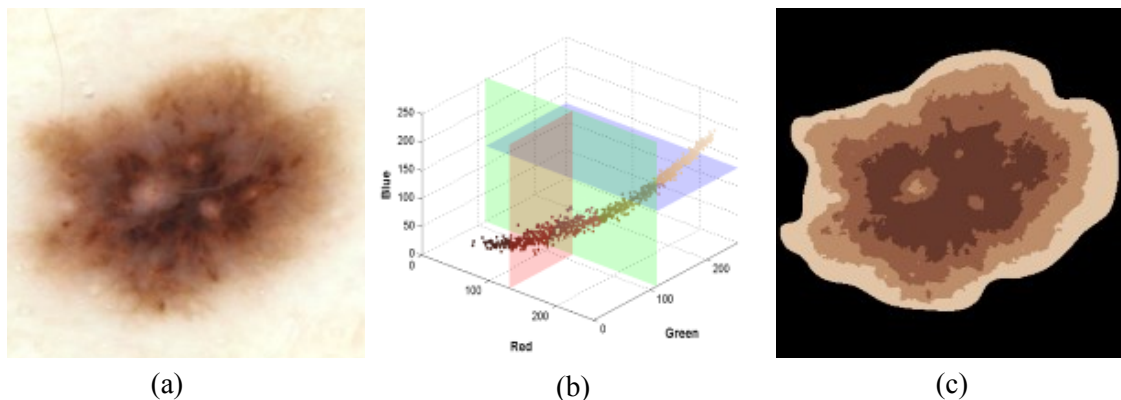
Figure 6. Median split segmentation performed by subsequent splitting of the plane with highest range. (a) Original dermoscopy image, (b) Histogram, (c) Median split image.

3.2.4. Pink Area. Menzies, et al., Stoecker, et al. and Rader, et al. have noted the importance of pink areas in dermoscopy images of melanoma [21-23]. In order to generate pink area related features, three different shades of pink; light, dark and pink-orange are segmented in a dermoscopy image. Figure 7 show different shades of pink along with the quintile overlay. It has been determined that the location of pink areas, particularly in the paracentral regions, has greater weight than the number of shades [24]. The three different shades of pink and quintile overlay derived from the distance transform are used to measure color, texture and blob features [24].
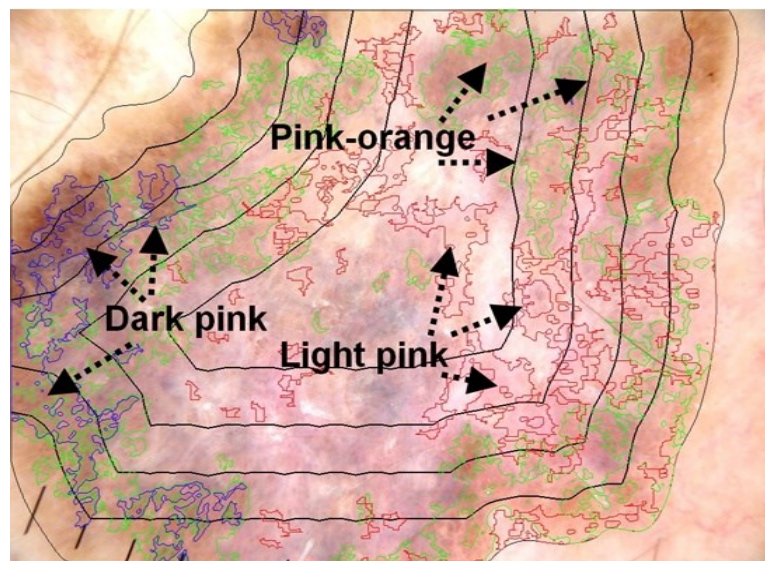
Figure 7. Automatically detected pink areas using 3-shade analysis, lesion quintile map overlaid [25].

3.2.5. Salient Points. The motivation for including salient point features in this research comes from the point that atypical pigments are critical in determining melanoma and these points are good representatives of such pigments. Salient points are detected using Steger's method of line detection [26]. The best results in terms of melanoma discrimination were obtained by using the intensity plane (R+G+B)/3 for detecting salient points [27]. The choice of sigma in the Gaussian filter, used for blurring as a pre-processing step, also affected the outcome and its optimal value was 1.02 [27]. Salient points determined in this way using the intensity plane were then used to calculate various texture and color features for aiding in the determination of melanoma. Figure 8 shows a sample salient point mask obtained from a dermoscopy image.

(a)   (b)
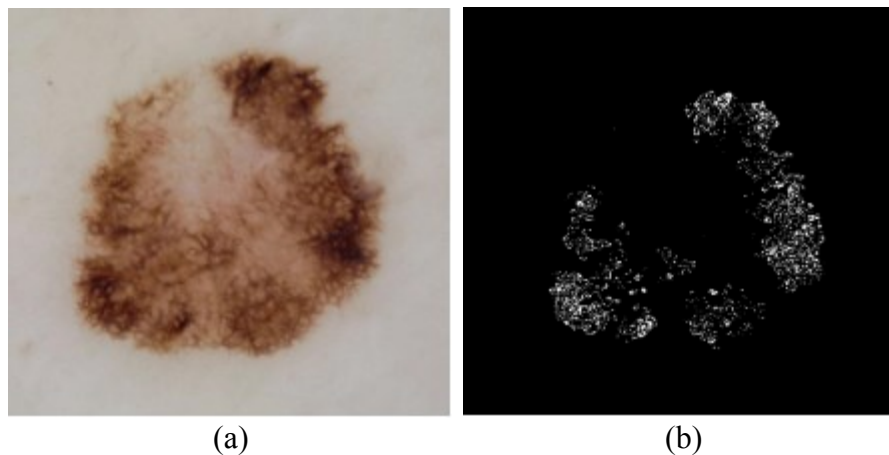
Figure 8. Sample of salient point image. (a) Original dermoscopy image, (b) Salient point mask.

4. DATA SET ACQUISITION AND DESCRIPTION

Skin lesion images used in this research are acquired from four clinic locations in the United States of America. These are contact non-polarized dermoscopy images taken using similar devices under similar lighting conditions and at the same magnification level. All images are RGB color images and are of size 768 by 1024.

This image data is divided into two sets; a training set and a test set. The training set consists of 837 lesion images with 184 melanomas and 653 benign lesions. The test set consists of 804 lesion images with 189 melanomas and 615 benign lesions. The lesion border masks for these images are manually acquired for this research. An automatically generated hair mask is used in the pre-processing.

5. CLASSIFICATION RESULTS AND DISCUSSION

The classification method in this research is based on logistic regression implemented in SAS (SAS Institute Inc., 100 SAS Campus Drive, Cary, NC 27513-2414, USA). Chi-square statistic is used as a measure of feature selection for the classifier model. A stepwise selection procedure is used for the logistic regression. Table 2 categorizes features being used in this research for the discrimination of melanoma from benign lesions.

Table 2. Number of features in each category.

Feature Category	Number of features
Clinical Features	9
APN Features	52
Median Split Features	265
White Area Features	437
Pink Area Features	161
Salient Point Features	7

The training and testing for the classification of melanoma are performed in a hierarchical manner and are examined in six different combinations by applying feature fusion. Fusion of clinical and dermoscopy features has been shown to provide enhanced discrimination of basal cell carcinoma (BCC), compared to using either clinical or dermoscopy features separately [28]. Results are presented for all the six combinations applied in this result. In the first combination, a model is built for each feature category and the output of that model is used to build the final model for classification. In the second combination, a model is built using white area features only and that is used along with other category features to build the final model. In the third combination, white area and pink area features are used separately to build their respective models and their outputs are used along with other category features to create the final model. In the fourth combination, separate models are built for APN features, for white area features and for pink area features and the outputs of those are combined with other remaining category features to build a final melanoma predicting model. The fifth combination has separate

models built from median split features, from white area features and from pink area features. Outputs from these models are used along with APN features, salient point features and clinical features to create a final prediction model. Finally, in the sixth combination separate models are built for everything except salient point features and clinical features. These models are then combined with salient point features and clinical features to build a final model to predict melanoma.

Table 3 summarizes the results for all six hierarchical combinations of features indicating the sensitivity and specificity for the training and test sets for each combination. It can be seen that the sensitivity for the training set is around 99% for each combination with the highest specificity of 76.88% obtained for third combination where white area and pink area models are combined with other feature categories for final melanoma prediction. This combination is also the best in terms of overall accuracy on the training set. A maximum sensitivity of 89.95% is achieved for the test set by implementing model from the second feature combination set, although in this case the specificity achieved is only 45.04%. With an intention of maximizing the sensitivity, the highest specificity achieved for the test set is 57.24%, which is for the fifth feature combination set. Table 3 also list area-under-the-cure (AUC) values for the training set for each feature combination set. The AUC is also referred to as an index of accuracy and is a performance metric for a receiver operating characteristic (ROC) curve which is a standard technique for summarizing a classifier performance. A maximum AUC of 0.982 is achieved for the model from the third feature combination set which also provided the maximum accuracy with the training set. For the model, which provided the maximum accuracy with the test set, the AUC achieved is 0.971.

Table 3. Classifier results for each of the six hierarchical combinations.

Feature Set Combination	Image Data Set	Sensitivity (%)	Specificity (%)	Overall Accuracy (%)	Training AUC
First Combination	Train	98.36	72.43	78.14	0.964
	Test	87.83	47.8	57.21	
Second Combination	Train	98.36	59.11	67.74	0.954
	Test	89.95	45.04	55.6	
Third Combination	Train	99.46	76.88	81.84	0.982
	Test	78.84	56.26	61.57	
Fourth Combination	Train	98.36	67.69	74.43	0.970
	Test	86.77	48.29	57.34	
Fifth Combination	Train	98.36	76.57	81.36	0.971
	Test	81.48	57.24	62.94	
Sixth Combination	Train	98.36	70.29	76.46	0.970
	Test	89.42	45.85	56.09	

Table 4, Table 5, Table 6, Table 7, Table 8 and Table 9 list some of the significant features included in the model based on their chi-square score for each of the six combinations, respectively. It is observed that clinical features like age of the patient, geographic location of the patient and change observed in the skin lesion are significant features irrespective of the model. Output from the APN feature model is also observed as a significant feature in the final model whenever it is used as feature as in the first, the fourth and the sixth combination models. Similarly, the median split-based model output is also a significant feature in cases where it is used to create final model, as seen in the first, the fifth and the sixth combination models. Features based on pink area model appears to be another significant feature as seen in the third, the fourth and the fifth models. The white area-based model output is not observed as a top feature when APN,

or the median split based model outputs are used in final model creation. This suggests that white area model output is less significant than model outputs from APN, median split or even pink area in the final model, as observed from the third, the fourth, the fifth and the sixth combination models.

Table 4. List of significant features in the first hierarchical combination.

S.N.	Feature Name	Chi-Square Score
1	APN feature model output	430.5092
2	Clinical feature model output	132.7874
3	Median split feature model output	35.2983

Table 5. List of significant features in the second hierarchical combination.

S.N.	Feature Name	Chi-Square Score
1	White area feature model output	211.7836
2	Age of the patient	118.2196
3	Geographic location of the patient	42.5898
4	Change observed in skin lesion	53.8852
5	Ratio of lesion perimeter to square-root of lesion area	13.3415

Table 6. List of significant features in the third hierarchical combination.

S.N.	Feature Name	Chi-Square Score
1	Pink area feature model output	245.4629
2	Age of the patient	123.6506
3	Geographic location of the patient	26.423
4	Change observed in skin lesion	28.0602
5	White are feature model output	19.6042

Table 7. List of significant features in the fourth hierarchical combination.

S.N.	Feature Name	Chi-Square Score
1	APN feature model output	430.5092
2	Age of the patient	71.3315
3	Change observed in skin lesion	20.2759
4	Geographic location of the patient	36.8922
5	Pink area feature model output	19.7516

Table 8. List of significant features in the fifth hierarchical combination.

S.N.	Feature Name	Chi-Square Score
1	Median split feature model output	408.5967
2	Age of the patient	67.704
3	Pink area feature model output	24.6514
4	Geographic location of the patient	20.9569
5	Change observed in skin lesion	15.6659

Table 9. List of significant features in the sixth hierarchical combination.

S.N.	Feature Name	Chi-Square Score
1	APN feature model output	430.5092
2	Median split feature model output	74.2869
3	Age of the patient	47.6047
4	Change observed in skin lesion	19.0427
5	Geographic location of the patient	32.6699

Figure 9 shows ROC curves for all six different models along with the area under the curve (AUC) values for each of them. An AUC value of more than 0.95 indicates good predictive power from each of the model.
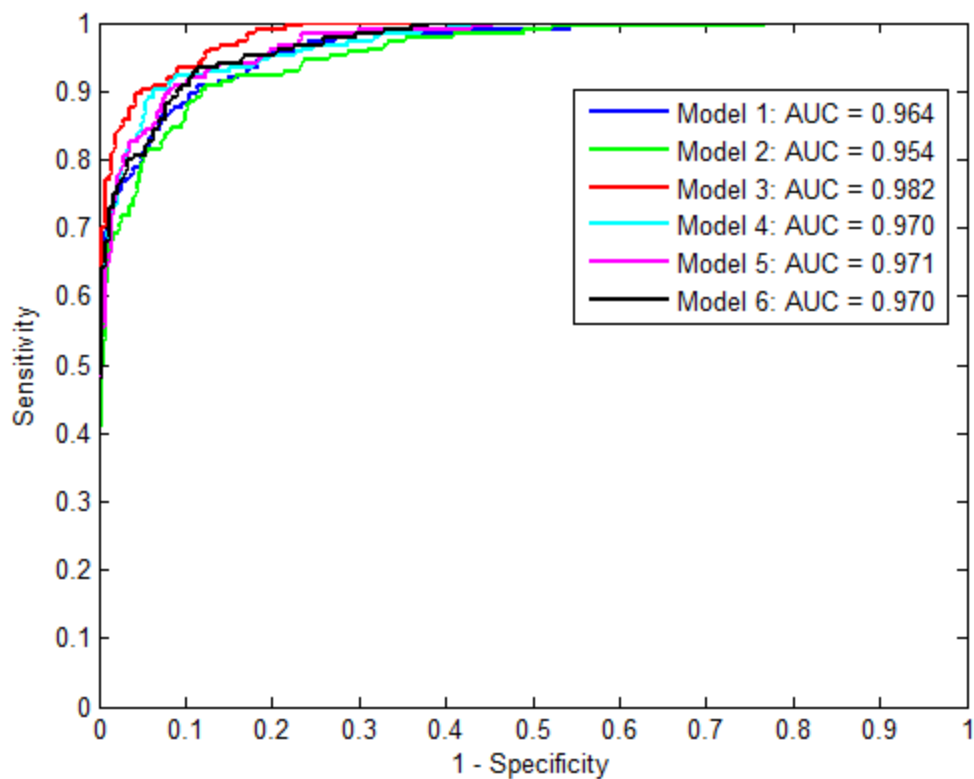

Figure 9. ROC curve for all six hierarchical combinations.

6. CONCLUSION

In this research, automatic classification of melanoma was performed using fusion of dermoscopy and clinical features. Various dermoscopy features, significant in determination of melanoma, were extracted after segmentation and their features were used along with clinical features in a logistic regression based classifier for discriminating melanoma from benign lesions. The disjoint training and test sets used in this research are real world data and are representative of the real world ratio of benign to melanoma.

Various combinations of features were used in hierarchical models and the third combination (white area model and pink area model outputs used along with other feature categories to build final model) provided the best result for the training set with sensitivity close to 99% and specificity of approximately 77%. The highest sensitivity achieved for the test set was approximately 90% for the second combination (white area model output used along with other feature categories) at which point the specificity was 45%. These results are promising given the size of the data set. It can also be observed that clinical features like age, change and location are significant in determining melanoma as are APN, median split and pink area features. Further experiments can be performed with other classifiers in order to explore more success with the existing features.

ACKNOWLEDGMENTS

REFERENCES

1. Siegel, Rebecca, Jiemin Ma, Zhaohui Zou, and Ahmedin Jemal. "Cancer statistics, 2014." *CA: A Cancer Journal for Clinicians* 64, no. 1 (2014): 9-29.

2. "The Cost of Cancer." National Cancer Institute at the National Institutes of Health. 2011. *http://www.cancer.gov/aboutnci/servingpeople/understandingburden/costof cancer.*

3. Pehamberger, Hubert, Michael Binder, Andreas Steiner, and Klaus Wolff. "In vivo epiluminescence microscopy: improvement of early diagnosis of melanoma." *Journal of Investigative Dermatology* 100 (1993): 356S-362S.

4. Soyer, H. Peter, Giuseppe Argenziano, Sergio Chimenti, and Vincenzo Ruocco. "Dermoscopy of pigmented skin lesions." *European Journal of Dermatology* 11, no. 3 (2001): 270-277.

5. Soyer, H. Peter, Giuseppe Argenziano, Renato Talamini, and Sergio Chimenti. "Is dermoscopy useful for the diagnosis of melanoma?" *Archives of Dermatology* 137, no. 10 (2001): 1361-1363.

6. Stolz, Wilhelm, Otto Braun-Falco, Peter Bilek, Michael Landthaler, Walter HC Burgdorf, and Armand B. Cognetta, eds. *Color Atlas of Dermatoscopy*. Wiley-Blackwell, 2002.

7. Braun, Ralph P., Harold S. Rabinovitz, Margeret Oliviero, Alfred W. Kopf, and Jean H. Saurat. "Pattern analysis: a two-step procedure for the dermoscopic diagnosis of melanoma." *Clinics in Dermatology* 20, no. 3 (2002): 236-239.

8. Boldrick, Jennifer C., Christle J. Layton, Josephine Nguyen, and Susan M. Swetter. "Evaluation of digital dermoscopy in a pigmented lesion clinic: clinician versus computer assessment of malignancy risk." *Journal of the American Academy of Dermatology* 56, no. 3 (2007): 417-421.

9. Perrinaud, A., O. Gaide, L. E. French, J-H. Saurat, A. A. Marghoob, and R. P. Braun. "Can automated dermoscopy image analysis instruments provide added benefit for the dermatologist? A study comparing the results of three systems." *British Journal of Dermatology* 157, no. 5 (2007): 926-933.

10. Perona, Pietro, and Jitendra Malik. "Scale-space and edge detection using anisotropic diffusion." *IEEE Transactions on Pattern Analysis and Machine Intelligence,* 12, no. 7 (1990): 629-639.

11. Argenziano, Giuseppe, Gabriella Fabbrocini, Paolo Carli, Vincenzo De Giorgi, Elena Sammarco, and Mario Delfino. "Epiluminescence microscopy for the diagnosis of doubtful melanocytic skin lesions: comparison of the ABCD rule of dermatoscopy and a new 7-point checklist based on pattern analysis." *Archives of Dermatology* 134, no. 12 (1998): 1563-1570.

12. Argenziano, Giuseppe, H. Peter Soyer, Sergio Chimenti, Renato Talamini, Rosamaria Corona, Francesco Sera, Michael Binder, Lorenzo Cerroni, Gaetano De Rosa, Gerardo Ferrara, Rainer Hofmann-Wellenhof, Michael Landthaler, Scott W. Menzies, Hubert Pehamberger, Domenico Piccolo, Harold S. Rabinovitz, Roman Schiffner, Stefania Staibano, Wilhelm Stolz, Igor Bartenjev, Andreas Blum, Ralph Braun, Horacio Cabo, Paolo Carli, Vincenzo De Giorgi, Matthew G. Fleming, James M. Grichnik, Caron M. Grin, Allan C. Halpern, Robert Johr, Brian Katz, Robert O. Kenet, MD, Harald Kittler, Jürgen Kreusch, Josep Malvehy, Giampiero Mazzocchetti, Margaret Oliviero, Fezal Özdemir, Ketty Peris, Roberto Perotti, Ana Perusquia, Maria Antonietta Pizzichetta, Susana Puig, Babar Rao, Pietro Rubegni, Toshiaki Saida, Massimiliano Scalvenzi, Stefania Seidenari, Ignazio Stanganelli, Masaru Tanaka, Karin Westerhoff, Ingrid H. Wolf, Otto Braun-Falco, Helmut Kerl, Takeji Nishikawa, Klaus Wolff, Alfred W. Kopf. "Dermoscopy of pigmented skin lesions: results of a consensus meeting via the Internet. "*Journal of the American Academy of Dermatology* 48, no. 5 (2003): 679-693.

13. Dalal, Ankur, Randy H. Moss, R. Joe Stanley, William V. Stoecker, Kapil Gupta, David A. Calcara, Jin Xu, Bijaya Shrestha, Rhett Drugge, Joseph M. Malters, Lindall A. Perry. "Concentric decile segmentation of white and hypopigmented areas in dermoscopy images of skin lesions allows discrimination of malignant melanoma." *Computerized Medical Imaging and Graphics* 35, no. 2 (2011): 148-154.

14. Meka, Sindhu L, "White area analysis for detection of malignant melanoma." M.S. Thesis in Electrical Engineering, Missouri University of Science and Technology, Rolla, MO, USA, 2012.

15. Mishra, Nabin K., "Fusion of dermoscopy and clinical data for classification of melanoma." *3rd Quadrennial Automatic Skin Cancer Detection Symposium*, Rolla, MO, USA, 2013.

16. Umbaugh, Scott E. *Digital Image Processing and Analysis: Human and Computer Vision Applications with CVIPtools*. CRC press, 2010.

17. Heckbert, Paul. "Color image quantization for frame buffer display." *SIGGRAPH Proceedings of the 9th Annual Conference on Computer Graphics and Interactive Techniques* (1982): 297-307.

18. Rosendahl, Cliff, Alan Cameron, Ian McColl, and David Wilkinson. "Dermatoscopy in routine practice: 'Chaos and clues'." *Australian Family Physician* 41, no. 7 (2012): 482.

19. Umbaugh, Scott E., Randy H. Moss, and William V. Stoecker. "Automatic color segmentation of images with application to detection of variegated coloring in skin tumors." *Engineering in Medicine and Biology Magazine, IEEE* 8, no. 4 (1989): 43-50.

20. Ghantasala, Kaushik. "Feature extraction through median-split algorithm for melanoma detection." M.S. Thesis in Electrical Engineering, Missouri University of Science & Technology, Rolla, MO, USA, 2013.

21. Menzies, Scott W., Juergen Kreusch, Karen Byth, Maria A. Pizzichetta, Ashfaq Marghoob, Ralph Braun, Josep Malvehy, Susana Puig, Giuseppe Argenziano, Iris Zalaudek, Harold S. Rabinovitz, Margaret Oliviero, Horacio Cabo, Verena Ahlgrimm-Siess, Michelle Avramidis, Pascale Guitera, Peter Soyer, Giovanni Ghigliotti, Masaru Tanaka, Ana M. Perusquia, Gianluca Pagnanelli, Riccardo Bono, Luc Thomas, Giovanni Pellacani, David Langford, Domenico Piccolo, Karin Terstappen, Ignazio Stanganelli, Alex Llambrich, Robert Johr. "Dermoscopic evaluation of amelanotic and hypomelanotic melanoma." *Archives of Dermatology* 144, no. 9 (2008): 1120-1127.

22. Stoecker, William V. "Dermoscopy and the diagnostic challenge of amelanotic and hypomelanotic melanoma." *Archives of dermatology* 144, no. 9 (2008): 1207-1210.

23. Rader, Ryan K., Katie S. Payne, Uday Guntupalli, Harold S. Rabinovitz, Maggie C. Oliviero, Rhett J. Drugge, Joseph J. Malters, and William V. Stoecker. "The Pink Rim Sign: Location of Pink as an Indicator of Melanoma in Dermoscopic Images." *Journal of Skin Cancer* 2014 (2014).

24. Albano, Peter, Bijaya Shrestha, William V. Stoecker, Jason Hagerty, Kristen Hinton. "Explosion of pink colors in melanoma." 2012.

25. Stoecker, William V., Nabin K. Mishra, Robert W. LeAnder, Ryan K. Rader, and R.J. Stanley. "Automatic detection of skin cancer - current status, path for the future." *In Proceedings of VISAPP* (1). (2013): 504-508.

26. Steger, Carsten. "Extracting lines using differential geometry and Gaussian smoothing." *International Archives of Photogrammetry and Remote Sensing* 31 (1996): 821-826.

27. Jella, Pavani. "Pigment network extraction and salient point analysis." M.S. Thesis in Electrical Engineering, University of Missouri, Rolla, MO, USA, 2004.

28. Cheng, Beibei, R. Joe Stanley, William V. Stoecker, Sherea M. Stricklin, Kristen A. Hinton, Thanh K. Nguyen, Rayan K. Rader, Harold S. Rabinovitz, Margaret Oliviero, Randy H. Moss. "Analysis of clinical and dermoscopic features for basal cell carcinoma neural network classification." *Skin Research and Technology* 19, no. 1 (2013): e217-e222.

SECTION

2. CONCLUSION

This dissertation presents a novel approach of automatic lesion border selection for dermoscopy images from borders generated by different segmentation algorithms. This approach further increases the accuracy of lesion segmentation on a variety of skin lesions thereby assisting other feature extraction algorithms for automatic classification of melanoma. This dissertation also presents a method of segmenting APN structures in a dermoscopy skin lesion based on the red plane variance. Features from the segmented regions are used in automatic classification of melanoma. In addition, the dissertation also explores the automatic classification of melanoma using fusion of clinical and other dermoscopy features by building a hierarchical classifier using different combinations of features. The results from this research indicate that the accuracy of automatic segmentation of skin lesions can be improved by implementing a classifier to select a good lesion border among the various choices available. Also, by combining clinical and dermoscopy features at different levels, higher accuracy of melanoma classification can be achieved.

VITA

Nabin K. Mishra received his Bachelor of Engineering degree in Electronics and Communication Engineering from Pulchowk Campus, Institute of Engineering (IOE), Tribhuvan University, Kathmandu, Nepal, in 2004. He earned his Master of Science degree in Electrical Engineering from Southern Illinois University Edwardsville, Edwardsville, IL, USA, in 2009. He began his Doctor of Philosophy degree in Electrical Engineering at Missouri University of Science & Technology, Rolla, MO, USA, in 2011. His research interests include machine learning, computational intelligence, image processing and data mining. He received his Doctor of Philosophy degree in Electrical Engineering from Missouri University of Science & Technology, Rolla, MO, USA, in 2014.